Correction of real-time satellite precipitation with satellite soil moisture observations

Wang Zhan[1], Ming Pan[1], Niko Wanders[1,2], Eric F. Wood[1]

[1] Department of Civil and Environmental Engineering, Princeton University, Princeton, NJ, USA

[2] Department of Physical Geography, Utrecht University, Utrecht, the Netherland

Abstract

Rainfall and soil moisture are two key elements in modeling the interactions between the land surface and the atmosphere. Accurate and high-resolution real-time precipitation is crucial for monitoring and predicting the on-set of floods, and allows for alert and warning before the impact becomes a disaster. Assimilation of remote sensing data into a flood-forecasting model has the potential to improve monitoring accuracy. Space-borne microwave observations are especially interesting because of their sensitivity to surface soil moisture and its change. In this study, we assimilate satellite soil moisture retrievals using the Variable Infiltration Capacity (VIC) land surface model, and a dynamic assimilation technique, a particle filter, to adjust the Tropical Rainfall Measuring Mission Multi-satellite Precipitation Analysis (TMPA) real-time precipitation estimates. We compare updated precipitation with real-time precipitation before and after adjustment and with NLDAS gauge-radar observations. Results show that satellite soil moisture retrievals provide additional information by correcting errors in rainfall bias. The assimilation is most effective in the correction of medium rainfall under dry to normal surface condition; while limited/negative improvement is seen over wet/saturated surfaces. On the other hand, high frequency noises in satellite soil moisture impact the assimilation by increasing rainfall frequency. The noise causes larger uncertainty in the

27 false-alarmed rainfall over wet regions. A threshold of 2 mm/day soil moisture change is

28 identified and applied to the assimilation, which masked out most of the noise.

29

30

31 **1 Introduction**

32 Precipitation is perhaps the most important variable in controlling energy and mass fluxes

33 that dominate climate and particularly the terrestrial hydrological and ecological systems.

34 Precipitation estimates, together with hydrologic models, provide the foundation for

35 understanding the global energy and water cycles (Sorooshian, 2004; Ebert et al., 2007).

36 However, obtaining accurate measurements of precipitation at regional to global scales

37 has always been challenging due to its small-scale, space-time variability, and the sparse

38 networks in many regions. Such limitations impede precise modeling of the hydrologic

39 responses to precipitation. There is a clear need for improved, spatially distributed

40 precipitation estimates to support hydrological modeling applications.

41 In recent years, remotely sensed satellite precipitation has become a critical data source

42 for a variety of hydrological applications, especially in poorly monitored regions such as

43 sub-Saharan Africa due to its large spatial coverage. To date, a number of fine-scale,

44 satellite-based precipitation estimates are now in operational production. One of the most

45 frequently used is the Tropical Rainfall Measuring Mission Multi-satellite Precipitation

46 Analysis (TMPA) product (Huffman et al., 2007). Over the 17 years lifetime since the

47 launch of the Tropical Rainfall Measuring Mission (TRMM) in 1997, a series of high

48 resolution (0.25-degree and 3-hourly), quasi-global (50°S - 50°N), near-realtime,

49 TRMM-based precipitation estimates have been developed and made available to the

50 research and applications communities (Huffman et al., 2007; 2010). Flood forecasting

51 and monitoring is one major application for real time satellite rainfall products (Wu et al,

52 2014). However, the applicability of satellite precipitation products for near real-time

53 hydrological applications that include drought and flood monitoring has been hampered

54 by their need for gauge-based adjustment.

55   While it is possible to create such estimates solely from one type of sensor, researchers

56   have increasingly moved to using combinations of sensors in an attempt to improve

57   accuracy, coverage and resolution. A promising avenue for rainfall correction is through

58   the assimilation of satellite-based surface soil moisture into a water balance model (Pan

59   and Wood, 2006). Over land, the physical relationship between variations in soil water

60   storage and rainfall accumulation contain complementary information that can be

61   exploited for the mutual benefit of both types of products (Massari et al., 2014; Crow et

62   al., 2009). Unlike instantaneous rain rate, satellite surface soil moisture retrievals utilize

63   low frequency microwave signals and possess some memory reflecting antecedent

64   rainfall amounts.

65   Studies have demonstrated that in situ (Brocca et al., 2009, 2013; Matgen et al., 2012)

66   and satellite (Francois et al., 2003; Pellarin et al., 2008, 2013; Brocca et al., 2014)

67   estimates of surface soil moisture could contribute to precipitation estimates by providing

68   useful information concerning the sign and magnitude of antecedent rainfall

69   accumulation errors. In particular, Brocca et al. (2014) estimated daily rainfall on a global

70   scale based on satellite SM products by inverting the soil water balance equation. Crow et

71   al. (2003, 2009, 2011) corrected space-borne rainfall retrievals by assimilating remotely

72   sensed surface soil moisture retrievals into an Antecedent Precipitation Index (API) based

73   soil water balance model using a Kalman filter (Kalman, 1960). However, these studies

74   focused on multi-day aggregation periods and a space aggregated correction at 1º

75   resolution for the corrected precipitation totals. This limits their applicability in

76   applications such as near real-time flood forecasting. Wanders et al. (2015) tried to

77   overcome this limitation by the correction of 3 hourly satellite precipitation totals with a

78   set of satellite soil moisture and land surface temperature observations. One important

79   conclusion by Wanders et al. (2015) is that their results showed the limited potential for

80   satellite soil moisture observations for correcting precipitation if "all-weather" – i.e.

81   microwave based – land surface temperatures are available coincidently and at high

82   spatial resolution as was the case with AMSR-E.

83   But this isn't always the case, and it is also noted that current low-frequency microwave

84   soil moisture missions (specifically SMAP and SMOS) don't have radiometers at

85   frequencies useful for estimating land surface temperatures, even though a 37 GHz sensor

86   is part of the AMSR2 system. In fact SMAP and ECMWF/SMOS use LST from weather

87   models analysis fields in their algorithms. Unfortunately the lowest microwave frequency

88   of AMSR2 and SMOS precludes retrieving soil moisture from many areas with heavy

89   vegetation, and AMSR2 has a significant dry bias with less availability than AMSR-E,

90   but is no longer operable. So improvements to satellite precipitation from the Global

91   Precipitation Mission products must reply solely on satellite soil moisture products from

92   SMAP, which is promises better soil moisture retrievals due to increased penetration

93   depth, and the improvements to the assimilation algorithms is the goal of this study.

94   Thus, we focus exclusively on the usefulness of assimilating soil moisture products to

95   improve satellite rainfall. We propose as part of the work how to improve the generation

96   of rain particles and the bias-correction of the satellite soil moisture observations, as well

97   as to enhance the assimilation algorithm to maximize the information that can be gained

98   from using soil moisture alone to adjust precipitation. Due to the very strong and

99   complicated spatial structure of precipitation, that is non-Gaussian and non-stationary in

100 both time and space (Wanders et al., 2015), a more advanced method is applied to

101 generate possible precipitation fields than were used in earlier studies or in Wanders et al,

102 2015) (see section 2.2.2). Furthermore, a more advanced bias correction method is also

103 applied to account for the reported problems in the second order statistics of the soil

104 moisture retrievals. We used a soil moisture remote sensing product to improve real-time

105 remote sensing precipitation product, TMPA 3B42RT, through a Particle Filter (PF) and

106 therefore offer an improved basis for quantitatively monitoring and predicting flood

107 events, especially in those parts of the world where in-situ networks are too sparse to

108 support more traditional methods of hydrologic monitoring and prediction. The

109 precipitation enhancement experiments are carried out over the continental U.S.

110 (CONUS) and the precipitation skill is validated against the NLDAS gauge-radar

111 precipitation product. Section 5 presents a comparison of the results from this study to

112 the earlier studies related to improving satellite precipitation.

2 Methods

2.1 Overview

Random replicates of satellite precipitation are generated based on real-time TMPA (3B42RT) retrievals and its uncertainty (Pan et al., 2010), which are then used to force the VIC land surface model (LSM) where one output of interest is surface soil moisture. Satellite soil moisture data products are compared and merged with the 3B42RT product to improve the accuracy of the satellite precipitation estimates. A schematic for the study approach is provided in Figure 1. Based on real-time 3B42RT retrievals, a set of possible precipitation estimates (a.k.a. replicates or particles) $\{p^i\}_{i=1,2,...,N}$ is generated with assigned initial prior probability weights $\{w^i\}_{i=1,2,...,N}$. These rainfall rates are then used to force the VIC land surface model to produce soil moisture predictions $\{\theta^i\}_{i=1,2,...,N}$. Retrievals of AMSR-E satellite surface soil moisture using the Land Surface Microwave Model (LSMEM) (Pan et al., 2014) are then merged with the LSM-based soil moisture within the Particle Filter (PF) that compares AMSR-E/LSMEM changes in soil moisture, ΔSM, to the LSM predicted soil moisture changes. From these, posterior weights $\{w^{i+}\}_{i=1,2,...,N}$ are calculated for each precipitation member (particle) that takes into account the uncertainties of AMSR-E/LSMEM ΔSM retrievals. From these updated weights, an updated precipitation probability distribution is constructed, where the precipitation particle with highest probability is taken as the "best" adjusted precipitation estimate (3B42RT$_{ADJ}$). The procedure is carried out over the continental US (CONUS) region on a grid-by-grid basis (0.25-degree) and a daily time step. Allowing for 6 months model spin-up period, the adjustment is done from January 2003 to July 2007.

2.2 Modeling, Statistical Tools and Data Sources

2.2.1 The Particle Filter

Data assimilation methods are capable of dynamically merging predictions from a state equation (i.e. the land surface model) with measurements (i.e. AMSR-E retrievals) to minimize uncertainties from both the predictions and measurements. It is assumed that

140 the source of uncertainty in the land surface model predictions come solely from the real-
141 time satellite precipitation, so that the particle filter (PF) provides an algorithm to update
142 the precipitation based on the AMSR-E retrievals. The state evolution of a particle filter
143 from discrete time t-1 to t can be represented as:

144 $$\theta_t = f_t(\theta_{t-1}, p_t, \kappa_t, \alpha_t) \tag{1}$$

145 where θ_t is the 1st layer soil moisture at time t, whose value is predicted by the state
146 equation Eq.(1) as $f_t(\bullet)$, and in the study is the hydrological model VIC, which takes in
147 forcing data, including precipitation (p_t) and other forcings (κ_t); and simulates land
148 surface states (soil moisture and soil temperatures at various levels, snow, etc.) and fluxes
149 (evapotranspiration, runoff) at time t. Herein we are basically interested only in the 1st
150 layer (top 10cm) soil moisture state and precipitation forcing, so other states and fluxes
151 are not explicitly shown. α_t is the random error in the prediction of θ_t, whose statistics
152 are known but not its value at any specific time.

153 At time t, the satellite surface soil moisture retrieval, θ_t^*, can be related to the VIC
154 modeled 1st layer soil moisture θ_t as:

155 $$\theta_t^* = h_t(\theta_t, \beta_t) \tag{2}$$

156 where h_t is taken as a regression that transforms the VIC simulated   1st layer soil
157 moisture to satellite surface soil moisture. β_t is the noise in this regression relationship.
158 The two noises α_t and β_t are assumed to be independent of each other at all times t.

159 At time t, given a 3B42RT precipitation estimate, p_t^{sat}, a set of N precipitation replicates
160 $\{p_t^i\}_{i=1,2,...,N}$ and their associated initial prior probability weight $\{w_t^i\}_{i=1,2,...,N}$ are
161 generated.

162 $$g(p_t^{sat}) \sim \{p_t^i, w_t^i\}_{i=1,2,...,N} \tag{3}$$

163 $$\sum_{i=1}^{N} w_t^i = 1 \tag{4}$$

164 g( ) is a probability density function. For N precipitation replicates, $\{p_t^i\}_{i=1,2,...,N}$, the
165 propagation of the states from time step (t-1) to t is by the VIC land surface model

166 represented in Eq.(1). The VIC land surface model simulates the 10cm 1st layer soil

167 moisture, $\{\theta_t^i\}_{i=1,2,...,N}$ for each precipitation replicate.

168 $$\{\theta_t^i = f_t(\theta_{t-1}, p_t^i, \kappa_t, \alpha_t)\}_{i=1,2,...,N} \tag{5}$$

169 with the associated weights assigned to the precipitation member:

170 $$\{\theta_t^i, w_t^i\}_{i=1,2,...,N} = \{f_t(\theta_{t-1}, p_t^i, \kappa_t, \alpha_t), w_t^i\}_{i=1,2,...,N} \tag{6}$$

171 If the satellite soil moisture retrieval at time t is θ_t^*, the update of precipitation forcing is

172 accomplished by updating the importance weight of each replicate given the

173 "measurement" θ_t^*:

174 $$w_t^{i+} \sim \{g(\theta_t^i | \theta_t^*)\}_{i=1,2,...,N} \tag{7}$$

175 $$\sum_{i=1}^{N} w_t^{i+} = 1 \tag{8}$$

176 The likelihood function $g(\theta_t^i | \theta_t^*)$ can be derived from h_t and $g(\beta_t)$. The schematic of the

177 utilized strategy is shown in Figure 2. The primary disadvantage of the particle filter is

178 the large number of replicates required to accurately represent the conditional probability

179 densities of p_t and θ_t. When the measurements exceed a few hundred, the particle filter is

180 not computationally practical for land surface problems. Considering computation

181 efficiency, we set the number of independent particles, N, from the prior distribution to

182 be 200.

183 **2.2.2 Precipitation Replicates Generation**

184 We generate precipitation replicates, $\{p_t^i\}_{i=1,2,...,N}$, based on statistics comparing NLDAS

185 and 3B42RT precipitation, as shown in Figure 3. Given a 3B42RT precipitation

186 measurement (binned by magnitude), with bin minimum and maximum indicated in

187 Figure 3, precipitation replicates are generated based on the corresponding 15th, 30th, 70th,

188 85th percentiles and the maximum NLDAS precipitation of the particular quantile bin as

189 follows: 15% of the replicates are generated with values uniformly distributed from 0 and

190 15th percentile; 15% of replicates with values from 15th to 30th percentile; 20% of

191 replicates with values from 30th percentile to the median; 20% of the replicates generated

192 from the median to 70th ; 15% with values from 70th to 85th percentile; and 15% from the

7

193 85th percentile to the maximum precipitation value. Note that although the generation of

194 particles is based on statistics calculated from NLDAS, results show little difference

195 generating precipitation ensembles uniformly distributed between 0 and 200 mm/day.

196 2.2.3 AMSR-E/LSMEM Soil Moisture Retrievals

197 The soil moisture product is derived from multiple microwave channels of the Advanced

198 Microwave Scanning Radiometer for EOS (AMSR-E) instrument. The retrieval algorithm

199 by Pan et al. (2014) is an enhanced version of the Land Surface Microwave Emission

200 Model (LSMEM). The near surface soil moisture and vegetation optical depth (VOD) are

201 estimated simultaneously from a dual polarization approach that utilizes both horizontal

202 (H) and vertical (V) polarizations measurement by the space-borne sensor. The input

203 AMSR-E brightness temperature comes from the NSIDC AMSR-E/Aqua Daily Global

204 Quarter-Degree Gridded Brightness Temperatures product (overlapping swaths in the

205 same day are truncated so that only the latest one is present). Consequently, the soil

206 moisture retrievals are also gridded at 0.25-degree with one ascending map and one

207 descending map at the daily time step. A maximum threshold value of 0.6 m^3/m^3 has been

208 applied manually to reduce error from open water bodies. According to Pan et al. (2014),

209 the soil moisture dataset based on observations from AMSR-E are shown to be consistent

210 at large scales in terms of reproducing the spatial pattern of soil moisture from VIC land

211 surface model simulation. Ascending soil moisture retrievals (equatorial crossing time

212 1:30PM local time) is assimilated in this study.

213 Similarly, while the spatial patterns of the basic statistics of AMSR-E/LSMEM SM

214 retrievals compare well to VIC simulations (Pan et al., 2014), VIC has its top layer (10

215 cm), which is deeper than the detection depth of AMSR-E, so that the mean and temporal

216 variability of the retrievals are higher than the VIC simulated soil moisture (Figure 4 in

217 Pan et al., 2014). Considering this difference between detection depths, we pre-process

218 soil moisture retrievals as follows:

219 1) Rescale soil moisture retrievals (AMSR-E/LSMEM SM) to have the same minimum

220 and maximum range as VIC simulated 1st layer soil moisture.

221   2) Calculate a daily soil moisture change. As satellite retrievals are manually truncated to

222   be no more than 0.6 m^3/m^3 (equivalent to 60mm of water in the top soil layer in VIC),

223   retrievals larger than 0.6 m^3/m^3 are excluded.

224   3) Fit a 2nd order polynomial regression model with ΔSM (all units in mm of water in the

225   top layer) from satellite and VIC simulation on a monthly basis and 3×3 grid scale

226   (window).

227   After pre-processing, the distribution of soil moisture change matches fairly well with

228   ΔSM$_{VIC}$ (Figure 4). The mean absolute difference reduces from a spatial average of 5.25

229   mm/day to 0.71 mm/day, with relatively larger value over eastern CONUS. According to

230   Pan et al. (2014), the no-skill or negative-skill areas occur mostly over eastern dense

231   forests due to vegetation blockage of the soil moisture signal (Pan et al., 2014). The

232   accuracy of soil moisture retrievals is also limited by mountainous topography and the

233   occurrence of snow and frozen ground during winter whose identification from satellite

234   observations is often difficult. For the purpose of this study, we assign zero weight to the

235   3B42RT$_{ADJ}$ and rely exclusively on the initial 3B42RT precipitation for time steps when

236   the VIC model predicts snow cover or frozen surfaces.

237   **2.2.4 VIC Land Surface Model**

238   The Variable Infiltration Capacity (VIC) model (Liang et al., 1994; Gao et al., 2010) is

239   used to dynamically simulate the hydrological responses of soil moisture to precipitation,

240   surface radiation and surface meteorology. The VIC model solves the full energy and

241   water balance over each 0.25-degree-grid-cell independently, thus ensuring its

242   computational efficiency. The assumption of independency poses limitation on the

243   application of LSM at very high spatial resolution (e.g. 1km×1km) over large areas.

244   Three-layer-soil-moisture is simulated through a soil-vegetation-atmosphere transfer

245   (SVAT) scheme, which also accounts for sub-grid scale heterogeneity of vegetation, soil

246   and topography. A detailed soil moisture algorithm description can be found in Liang et

247   al. (1996). The VIC model has been validated extensively over CONUS by evaluating

248   soil moisture and simulations to observations (Robock et al., 2003; Schaake et al., 2004).

3 Idealized Experiment

Before applying the Particle Filter assimilation algorithm on 3B42RT precipitation estimates, we conducted an idealized experiment where we treat the NLDAS precipitation as the "truth" and the NLDAS precipitation forced VIC simulations as "satellite observed" soil moisture. As an idealized experiment, we adjust TMPA real-time precipitation estimates based on these "satellite observations". Phase 2 of the North American Land Data Assimilation System (NLDAS-2) rainfall forcing combines hourly WSR-88D radar analyses from the National Weather Service (NWS) and daily gauge reports (~13,000/day) from the Climate Prediction Center (CPC) (Ek et al., 2011). The dataset, with a spatial resolution of 0.125 degree and hourly observations, was pre-processed into 0.25-degree daily precipitation to be consistent with that of 3B42RT and AMSR-E/LSMEM SM datasets. Hourly NLDAS and 3-hourly 3B42RT precipitation is aggregated into daily precipitation defined by a period shifted ~7.5 hours into the future (9:00PM-9:00PM), allowing for a necessary delay for soil moisture to respond to incoming rainfall. The idealized experiment is designed to test whether the algorithm is able to retrieve rainfall forcing with soil moisture change, assuming that the soil moisture observations are 100% accurate.

Results show that, with the knowledge of 1st layer soil moisture change (via the "satellite observations"), the adjustment is able to recover intensity and spatial pattern of forcing precipitation (Figure 5g). Average mean absolute error (MAE) of daily rainfall amount is reduced by 52.9% (2.91 mm/day to 1.37 mm/day) over the region. Figure 5a to Figure 5e shows an example of the recovered rainfall field from the idealized experiment for 27th Oct. 2003. The spatial pattern matches the original NLDAS precipitation well.

3.1 Effect of surface soil saturation

While successfully recovering the general pattern of NLDAS precipitation based on first layer soil moisture, the idealized experiment is not always able to recover the precipitation volume due to the fact that the top layer soil moisture alone does not contain the complete memory of the previous day's rainfall. Deeper soil moisture, evapotranspiration and runoff also carry part of this information. As the surface gets

10

278   wetter, the VIC 1st layer soil moisture has smaller variation. If the incoming precipitation

279   brings the surface to saturation, the VIC model redistributes the soil moisture vertically

280   though vertical moisture flow and generates runoff. Hence soil moisture increments,

281   ΔSM, near saturation are less correlated with incoming precipitation as they change

282   minimally to additional incoming rainfall. An example demonstrating this saturation

283   effect is shown in Figure 5f to Figure 5j. When incoming precipitation brings the surface

284   SM to (near) saturation, there is very limited improvement after the adjustment. Because

285   of the low sensitivity of the soil surface to precipitation, there is little change in ΔSM in

286   response to precipitation variations among the replicates. It is almost always the case that

287   the algorithm is not able to find a "matching" ΔSM.

288   We separately evaluate the skill improvement in the recovered NLDAS precipitation with

289   and without surface saturation. Figure 6 confirms the effect of surface saturation on

290   adjusted precipitation, which is well described in previous studies (e.g. Brocca et al.,

291   2013, 2014). The recovered precipitation, when the surface soil is saturated, only

292   contributes more noise rather than an improvement to the rainfall estimates. The VIC

293   model computes the moisture flow between soil layers using an hourly time step. If the 1st

294   layer soil moisture exceeds its maximum capacity, it is considered to be a surface

295   saturation case. As seen in Figure 5, there is very limited or negative skill in the

296   recovered precipitation under saturated surface soil moisture conditions. Such

297   circumstances are identified and the AMSR-E/LSMEM ΔSM observation disregarded by

298   assigning zero weight to the 3B42RT$_{ADJ}$ values. Thus for wetter areas with heavy

299   precipitation that potentially would bring the surface soil moisture to saturation, the

300   3B42RT product is less likely to be adjusted according to satellite ΔSM and the best

301   precipitation estimate is 3B42RT.

3.2 Effect of SM uncertainty

303   In the idealized experiment, NLDAS-VIC soil moisture is taken as truth with zero

304   uncertainty associated with (θ_t^*). However, this assumption is not valid for real satellite

305   SM retrievals, mean absolute error of which is approximately 3% vol./vol. (McCabe et

306   al., 2005). To consider this, we added error to the "truth" SM (normally distributed with

307   zero mean and standard deviations of 1mm, 2mm, 3mm, 4mm and 5mm), and simulated

308   the effect of SM uncertainty to evaluate the associated adjustment errors. Figure 7 shows

309   that larger soil moisture observation errors lead to larger error variation after adjustment.

310   This also suggests that soil moisture responds to precipitation non-linearly based on

311   different initial conditions. An estimated wetter surface has lower sensitivity to an

312   incoming rainfall amount, resulting in larger error in the recovered NLDAS precipitation.

313   As shown in Figure 7, the error standard deviation of the recovered NLDAS precipitation

314   increases with surface water content (statistics shown in Table 2). As we add noise larger

315   than N(0,1mm) into "true" SM observation, there is a wet bias of approximately 1

316   mm/day regardless of 1st layer soil moisture level. This suggests that when the difference

317   between 1st layer SM and saturation is less than 8 mm, the median of the errors in the

318   recovered NLDAS precipitation grows from 0.16 mm/day to 1.89 mm/day when we add

319   N(0,5mm) noise, while inter-quantile range (IQR) increases from 1.71 mm/day to 7.04

320   mm/day. Acknowledging such a wet bias, to avoid introducing any more unintentional

321   bias in the 3B42RT$_{ADJ}$ estimates, we take as zero the uncertainty of AMSR-E/LSMEM

322   SM retrievals, i.e. we take $h_t(\theta_{t,})$ as our single observation θ_t^* and adjust the 3B42RT

323   estimates accordingly.

324   It is noteworthy that the soil moisture change is calculated based on previous days' soil

325   water contents. Therefore errors tend to accumulate over time until they are "re-set" when

326   a significant precipitation event takes place. This type of uncertainty accounts for a small

327   portion of the total error in the adjusted precipitation (black being the no error case in

328   Figure 7 with the "true" change in soil moisture from every time step). As complete

329   global coverage is not provided with each orbit of the AMSR-E sensor, on average 44.01%

330   of the time steps (<0.6 m^3/m^3) during the study period have observations, with more

331   frequent overpasses at higher latitudes (Figure 4e in Pan et al., 2014). This observation

332   gap unavoidably introduces extra uncertainty in the retrieval of the precipitation signal.

333   To further avoid possible additional errors, we update the forcing rainfall when a ΔSM

334   temporal match (±0.4mm) is available, and keep the original precipitation if a match isn't

335   available.

4 Improvement on real-time precipitation estimates and their validation

The adjustment of real TMPA 3B42RT retrievals based on AMSR-E/LSMEM ΔSM is carried out using the methods described in Section 2.2.3, and results from the idealized experiment (Sect. 3) with regard to the circumstances where an adjustment is applied.

An example of TMPA 3B42RT adjustment is provide in Figure 8, where a snapshot of the rainfall field is shown (Figure 8b) and compared with NLDAS on May 26th 2006 and the adjusted rainfall pattern based on AMSR-E/LSMEM ΔSM. The 3B42RT$_{ADJ}$ rainfall field (Figure 8c) is similar in terms of its spatial distribution compared to NLDAS precipitation estimates (Figure 8d).

On average TMPA 3B42RT and AMSR-E/LSMEM ΔSM have a spatial Pearson Correlation Coefficient of 0.37 (Shown in Figure 9, left), compared to 0.52 for the correlation between NLDAS and ΔSM. After the adjustment procedure, the Pearson correlation coefficient between 3B42RT$_{ADJ}$ and AMSR-E/LSMEM ΔSM increases to 0.53 (shown in Figure 9), indicating that the correction method is successful. A below average increase in correlation is found over the western mountainous region, the Great Lakes region and eastern high vegetated and populated region. Additionally, the satellite soil moisture suffers from snow/ice/standing water contamination, which affects the potential for improved results after correction. The 3B42RT$_{ADJ}$ has significant improvement over 3B42RT in terms of long-term precipitation bias. The bias in 3B42RT annual mean precipitation is reduced by 20.6%, from -9.32mm/month spatial average in 3B42RT to -7.40mm/month in 3B42RT$_{ADJ}$ (shown in Figure 9, right). Frequency of rain days generally increases significantly everywhere (Figure 10). The NLDAS data (Figure 10, right) suggests an almost constant drizzling rainfall over parts of the western mountainous area (Montana, Idaho, Wyoming and Colorado), while assimilating AMSR-E/LSMEM ΔSM datasets does not have a signal of higher rainfall frequency (Figure 10, middle). This is possibly due to lower soil moisture variability in satellite retrievals over the dry, mountainous areas and frequent presence of snow and ice (3B42RT is not updated under such circumstances).

Figure 11 shows the assimilation results for the grids and days with soil moisture observations, using the NLDAS precipitation as a reference. Overall, the method is

13

366 successful in correcting daily rainfall amount when 3B42RT overestimates precipitation

367 (3B42RT - NLDAS > 0). Mean standard deviation (STD) of 3B42RT$_{ADJ}$–NLDAS is

368 between 1 and 3 mm/day (statistics provided in Table 3). When 3B42RT underestimates

369 rainfall (3B42RT - NLDAS < 0), the assimilation has limited improvement on 3B42RT.

370 This is due to the effect of surface saturation. In terms of adding rainfall, there are two

371 scenarios when the effectiveness of the assimilation is limited.

372 1) The presence of wet conditions or (near) saturation. There is higher probability

373   bringing the surface to saturation (wetter condition) when the assimilation adds

374   rainfall into 3B42RT. However soil moisture increments are less sensitive to

375   incoming precipitation on wetter soil. Therefore, an error in ΔSM often translates into

376   3B42RT$_{ADJ}$ in a magnified manner.

377 2) The presence of very heavy precipitation, which typically brings the surface to

378   saturation, hence not results in an update of 3B42RT, is not updated. If, by a small

379   probability, the surface is wet (nearly saturated) but not completely saturated after a

380   heavy rainfall, the updated 3B42RT also suffers from large uncertainty (explained in

381   1) above).

382 The effect of the assimilation conditioned on 3B42RT rainfall amount is further evaluated

383 by skill scores. Figure 12 presents probability of detection (POD) and false alarm rate

384 (FAR) in 3B42RT and 3B42RT$_{ADJ}$, using NLDAS as the reference dataset. The rain event

385 threshold is set to be 0.1 mm/day and 2 mm/day. This is possibly due to lower soil

386 moisture variability in satellite retrievals over the dry, mountainous areas and frequent

387 presence of snow and ice (3B42RT is not updated under such circumstances). For a 0.1

388 mm/day threshold, both FAR and POD increases in 3B42RT$_{ADJ}$ except for the

389 mountainous region. Whereas for a 2 mm/day threshold, there is only slight increase in

390 FAR in most of eastern U.S. region. The overestimation of rain days is also absent when

391 2 mm/day event threshold is applied which suggests that most of the excessive rainy days

392 have less than 2 mm/day rain amount. Consistent with other studies, spatially, larger

393 improvements are found in the central U.S. The area coincides where higher AMSR-

394 E/LSMEM ΔSM accuracy is found (non-mountainous regions with little urbanization and

395 light vegetation). Despite of the regional variability, these excessive rainy days are a

14

396 result of the high-frequency noise in AMSR-E/LSMEM soil moisture retrievals identified

397 by Pan et al (2004) and Wanders et al. (2015).

398 The applied method is ineffective for light rainfall < 2 mm, where the adjustment tends to

399 over-correct precipitation by adding excessive rainfall – mostly the result of the high

400 frequency AMSR-E noise. MAE of light rainfall (< 2 mm/day) increased from 0.65

401 mm/day in 3B42RT to 0.99 mm/day in $3B42RT_{ADJ}$. On the other hand, satellite soil

402 moisture assimilation is very effective in correcting satellite precipitation larger than 2

403 mm/day: MAE of medium to large rainfall (≥ 2 mm/day) decreased from 7.07 mm/day in

404 3B42RT to 6.55 mm/day in $3B42RT_{ADJ}$. The effect of the assimilation is different over

405 the western mountainous region, the north-to-south central U.S. band and the eastern U.S.

406 The western mountainous region has a dry climatology with more frequent rainfall in

407 small amounts. The white noise in ΔSM, negatively impacting $3B42RT_{ADJ}$, is comparable

408 to the positive improvement brought by actual light rainfall signals in ΔSM. Therefore,

409 the assimilation of ΔSM has no significant impact in these regions.

410 The north-to-south band over central U.S. experiences more medium to large (≥ 2

411 mm/day) rainfall. In addition, the region is lightly vegetated (annual mean LAI <1) with

412 low elevation (< 1500 m), where soil moisture retrievals are of higher accuracy. Soil

413 moisture climatology is wetter in the west, causing larger variations in $3B42RT_{ADJ}$ error

414 from the white noise ΔSM (as discussed in Section 3.2). Despite of that, satellite soil

415 moisture is most effective correcting medium to large rainfall under normal surface

416 conditions.

417 The decreased skill in $3B42RT_{ADJ}$ over eastern U.S. is primarily attributed to both

418 precipitation and soil moisture climatology, a wet climate with more medium to large

419 rainfall, neither of which is suitable for soil moisture assimilation.

420 In summary, the high-frequency noise in soil moisture product causes a major limitation.

421 The noise impacts adjusted precipitation by introducing false alarm rain days. It is

422 difficult to distinguish the noise and retrieve the true rainfall signals. A remedy to prevent

423 the excessive rain days is applying a cutoff ΔSM threshold when rain days are added, at

424 the expense of neglecting a part of the true rainfall signals. Figure 13 shows the

425 probability of added rainy days being consistent with NLDAS (NLDAS > 0 mm/day)

426 with respect to ΔSM. When a new rainy day is added (3B42RT = 0 mm/day, $3B42RT_{ADJ}$

427 > 0 mm/day) based on AMSR-E/LSMEM ΔSM of 2 mm/day, there's approximately 78%

428 chance that the added rain day is a true event (NLDAS > 0 mm/day); That is, approx.

429 22% chance that it is a false alarm (NLDAS = 0 mm/day). When AMSR-E/LSMEM

430 ΔSM is larger than 2 mm/day, the probability of added rainy days being true event is

431 even higher, up to 90% chance. Here we applied a threshold of 2 mm/day on AMSR-

432 E/LSMEM ΔSM. That is, when new rainy days are introduced (3B42RT > 0,

433 3B42RTADJ > 0), we discard the update and keep the no-rain day if AMSR-E/LSMEM

434 soil moisture increment is below 2 mm. Note that, the probability of the false alarms

435 depends on soil moisture climatology: the wetter soil moisture climatology, the larger

436 uncertainty in the signal. Therefore, this threshold should vary in accordance with local

437 soil moisture climatology, i.e. a larger threshold over the wetter east U.S. and smaller

438 threshold over the drier western U.S. Nevertheless, after the 2 mm/day ΔSM threshold is

439 applied, expectedly, the statistics are largely improved: FAR is decreased significantly

440 from 0.519 (wo. ΔSM threshold) to 0.066 (w. ΔSM threshold). MAE of light rainfall (< 2

441 mm/day) in $3B42RT_{ADJ}$ decreased from 0.99 mm/day to 0.64 mm/day, compared to 0.65

442 mm/day in 3B42RT. For medium to large 3B42RT rainfall (≥ 2 mm/day), it effectively

443 increased POD (0.362 in 3B42RT vs 0.386 in $3B42RT_{ADJ}$ w. ΔSM threshold) and

444 decreased FAR (0.037 in 3B42RT vs 0.030 in $3B42RT_{ADJ}$ w. ΔSM threshold). Further

445 work is needed to characterize, distinguish and decrease the high-frequency noise in SM

446 retrievals. Figure 13 gives an example of evaluating the impact of SM uncertainties in

447 assimilation as curves derived over different topography can be quantitatively compared.

448 **5 Comparison to other studies**

449 Many other studies have utilized satellite microwave brightness temperatures or soil

450 moisture retrievals to constrain satellite precipitation estimates (Pellarin et al., 2008),

451 estimate precipitation (e.g. Brocca et al., 2013) or improve precipitation estimates

452 through assimilation (Crow et al., 2009, 2011). Here, we review their approaches and

453 findings in light of the results of this study, and compare our results with some of these

454 studies to gain insight into their robustness and consistency.

455   Pellarin et al. (2008) used the temporal variations of the AMSR-E 6.7 GHz brightness

456   temperature (TB) normalized polarization difference, $PR=(TB_V-TB_H)/(TB_V+TB_H)$, to

457   screen out anomalous precipitation events from a 4-day cumulative satellite-estimated

458   precipitation (EPSAT-SG: Chopin et al., 2005) from 22 to 26 of June 2004 over a 100 x

459   125 km box centered over Niger in west Africa. This was extended in Pellarin et al.

460   (2013) where an API-based water balance model was used to correct three different

461   satellite precipitation products (CMORPH, TRMM-3B42 and PERSIANN) over a 4-year

462   period in west Africa at three 0.25° grids in Niger, Benin and Mali). The new algorithm

463   was evaluated by comparing the corrected precipitation to estimates over the 0.25° grids

464   from ground-based precipitation measurements. A sequential assimilation approach was

465   applied where AMSR-E C-band TB measurements were used to estimate a simple

466   multiplicative factor to the precipitation estimates in order to minimize the difference

467   between observed (AMSR-E) and simulated TBs in term of root mean square error

468   (RMSE). The results show improvements over those found in Pellarin et al. (2009).

469   Specifically, the Pellarin et al. (2013) study shows that the proposed methodology

470   produces an improvement of the RMSE at daily, decadal and monthly time scales and at

471   the three locations. For instance, the RMS mean error decreases from 7.7 to 3.5 mm/day

472   at the daily time scale in Niger and from 18.3 to 7.7 mm/day at the decadal time scale in

473   Mali.

474   Crow et al. (2003, 2009, 2011) demonstrated the effectiveness of the assimilation of

475   remotely sensed microwave brightness temperatures or retrieved soil moisture in

476   estimating precipitation based on airborne measurements over the Southern Great Plains

477   (USA) region (Crow et al., 2003); 2 to 10 day accumulated precipitation within a simple

478   API water budget model and assimilation scheme over CONUS (Crow et al., 2009); and

479   3 day, 1° precipitation accumulation over three African Monsoon Multidisciplinary

480   Analysis (AMMA) sites in west Africa with an enhanced assimilation scheme and an

481   API-moisture model (Crow et al., 2011). Crow et al. (2009) recommends against

482   estimating precipitation at a larger scale than three days based on assimilating AMSR-

483   E/LSMEM soil moisture.

484   Brocca et al. (2013) estimated precipitation by inverting the water budget equation such

485   that precipitation could be estimated from changes in soil moisture. The inverted equation

486   was calibrated using in-situ, 4-day averaged observations at two sites in Spain and Italy.

487   In Brocca et al. (2014), the same approach was used globally for 5-day precipitation

488   totals and at 1° spatially. Soil moisture observations from three satellite derived soil

489   moisture datasets (AMSR-E LPRM, ASCAT and SMOS) were used. The soil moisture

490   and rainfall were aggregated to a 1° spatial resolution, the soil moisture changes over a 5-

491   day period to estimate a 5-day total precipitation. No formal data assimilation was carried

492   out. The newly created precipitation data set was compared to two satellite precipitation

493   products (TRMM-3B42RT, GPCC) and two gauge based precipitation products (GPCP,

494   ERA-Interim). But they do note that their approach has "poor scores in reproducing daily

495   rainfall data". Nonetheless, these studies show promising results.

496   In the study reported here, three advances have been made over these earlier studies: (i)

497   we adopted a state-of-the-art dynamic land surface model that has demonstrated high skill

498   in simulating soil moisture when driven by high quality precipitation data (Schaake et al.,

499   2004); (ii) we applied a state-of-the-art data assimilation procedure based on particle

500   filtering so as to extract (and hopefully maximize) the information content from the

501   satellite most effectively; (iii) we increased the resolution of the precipitation estimation

502   window down to 1 day, exceeding the conclusions in these earlier studies that the finest

503   temporal resolution is 3 to 5 days. Additionally we increased (or matched) the spatial

504   resolution to 0.25°, limited primarily by the satellite soil moisture product resolution; and

505   (iv) previous studies are based on the assumption that the SM retrievals are 100%

506   accurate and contain no errors. We evaluated this assumption by analyzing the impact of

507   uncertainties associated with the soil moisture retrievals. These advances offer important

508   benefits when satellite precipitation products are used for applications such as flood

509   forecasting. Admittedly by aggregating in space and time, the improvement is more

510   robust since some errors are averaged out. However improving satellite precipitation by

511   AMSR-E/LSMEM SM is not entirely without skill. In fact, it could effectively correct

512   rainfall with proper cautions given to local climatology where the assimilation is carried

513   out.

514   Wanders et al. (2015) performed a comprehensive inter-comparison study using multiple

515   satellite soil moisture and land surface temperature (LST) data at fine temporal scale (3-

516   hourly). Compared to their study, ours focuses on using soil moisture exclusively from

18

517   one satellite and retrieval algorithm, and in improvements to the assimilation algorithm.

518   Specifically in (i) the longer temporal period (2010-2011 in Wanders, et al. versus 2002-

519   2007 in this study), (ii) the temporal resolution (3-hourly versus daily); (iii) the particle

520   generation and bias correction method. We present in the paper improvements in the

521   generation of rain particles and the bias-correction of the satellite soil moisture

522   observations, as well as enhancements to the assimilation algorithm to maximize the

523   information that can be gained from using soil moisture alone in adjusting precipitation.

524   Due to the very strong and complicated spatial structure of precipitation, that is non-

525   Gaussian and non-stationary in both time and space, a more advanced method is applied

526   to generate possible precipitation fields than used or presented in earlier studies or in

527   Wanders et al, (2015). Furthermore, a more advanced bias correction method is also

528   applied to account for the reported problems (Wanders et al., 2015) in the second order

529   statistics of the soil moisture retrievals; and (iv) SM retrieval products (and overpasses)

530   used in assimilation. Our improved results are based on soil moisture retrievals from

531   ascending overpasses only (versus both descending and ascending overpasses from

532   multiple datasets, i.e. AMSR-E/LSMEM, ASCAT and SMOS). Our exclusive focus on

533   the usefulness of soil moisture product promises more applicability especially for

534   improving satellite precipitation from the Global Precipitation Mission products. The

535   descending overpasses have generally better performance than the ascending, suggesting

536   the potentials of further improvements.

537   A quantitative comparison of Wanders et al. (2015) and our results is provided below.

538   Despite of the different time periods between Wanders et al. (2015, 2010-2011) and in

539   our study (2002-2007), Wanders et al. (2015) shows decreasing POD (-15.0% to -46.4%

540   depending on different products used) and FAR (-47.2% to -89.1% depending on

541   different products used) for all rainfall after assimilation using either (single or multiple)

542   SM products alone or SM + LST data combined (see Table 4 of Wanders et al., 2015).

543   While in our study, after applying ΔSM threshold, medium to large 3B42RT$_{ADJ}$ rainfall

544   ($\geq$ 2 mm/day) has an increase in POD (+6.6%) and decrease in FAR (-18.9%).

545   Furthermore, the significant dry bias in adjusted precipitation (see Fig.6 of Wanders et

546   al., 2015) is not present in our results (Figure 9). This is due to improvements in our

547   precipitation ensemble generation and bias correction scheme. Wanders et al. (2015)

19

548   applied an additional step generating precipitation particles sampling from a 3×3 window

549   that over-eliminates most of the excessive rainfall along with some real signal. We

550   suggest loosening this constraint to a larger window size or to sample from adjusted

551   precipitation instead of original 3B42RT precipitation. However sampling from adjusted

552   precipitation at each time step would significantly increase the computational demand,

553   limiting the potential for a global application at high temporal/spatial resolution.

554   Furthermore, the outcome is quite different for the distribution of soil moisture retrievals

555   after pre-processing (Fig.9 of Wanders et al. 2015 vs Figure 4 in our study) due to

556   different methods used. After pre-processing, distributions of soil moisture retrievals is

557   more similar to that of NLDAS precipitation forced, VIC modeled 1st layer soil moisture.

558   CDF-matching used by Wanders et al., (2015) is based on the assumption that satellite

559   soil moisture and modeled soil moisture respond to heavy rainfall in the same way –

560   essentially having a rank correlation of 1. However that is not observed because of

561   shallower detection depth of the satellite soil moisture. On the other hand, using the pre-

562   processing method presented in this study, the signal of near-saturation in AMSR-

563   E/LSMEM ΔSM tends to be overestimated after pre-processing, which indicates a heavy

564   rain event that is often accompanied with surface saturation and thus does not provide

565   effective information for the assimilation. The other benefit of the 2nd order polynomial

566   regression lies in its non-linearity. An error in the soil moisture product impacts the

567   precipitation adjustment in a predictable way, allowing for a more systematic post-

568   processing treatment. Based on the known error characteristics, we demonstrate a

569   potential remedy to deal with the error by applying a 2 mm/day cutoff ΔSM threshold.

570   Meanwhile, it is also highlighted that the cutoff threshold should be variable and

571   positively correlated with local soil moisture climatology. We acknowledge that the soil

572   moisture product used in Wanders et al. (2015), is a blended product of multiple satellite

573   soil moisture datasets. It is not clear how its error characteristics impact the adjusted

574   precipitation.

575   **6 Conclusion and Discussion**

576   Based on the retrieved soil moisture from AMSR-E using the LSMEM retrieval

577   algorithm, we propose an assimilation procedure to integrate soil moisture information

578   into the VIC land surface model so as to improve real-time, satellite precipitation

579   estimates. The ability to estimate rainfall amount is now enhanced with the above

580   improvements, especially for correcting medium rainfall amounts. However, constrained

581   by the noise in AMSR-E TBs and thus soil moisture retrievals, the assimilation is not

582   effective in detecting missed rainfall events. The improved precipitation estimates,

583   referred to as 3B42RT$_{ADJ}$ estimates, are overall consistent in reproducing the spatial

584   pattern and time series of daily rainfall from NLDAS precipitation. The results illustrate

585   the potential benefits of using data assimilation to merge satellite retrievals of surface soil

586   moisture into a land surface model forced with real-time precipitation. Potentially the

587   method can be applied globally for areas meeting vegetation cover and surface condition

588   constraints that allows for soil moisture retrievals. Under these conditions, the approach

589   can provide a supplementary source of information for enhancing the quality of satellite

590   rainfall estimation, especially over poorly gauged areas like Africa.

591   Nonetheless, some caution is required. The results of this study show that the adjusted

592   real-time precipitation tends to add additional rain (frequency) resulting in more time

593   steps with rain but lower regional average in the western U.S. and slightly higher regional

594   average in the eastern U.S. It is also noticed that the precipitation adjustments are

595   insensitive under saturated soil moisture conditions. A wetter surface magnifies any error

596   associated with satellite observation by incorrectly adjusting precipitation. These errors,

597   mixed with the "real" signal, generally add approximately ~2mm of precipitation (or

598   higher) depending on the soil moisture climatology. It is important to consider these

599   circumstances when observations are used so as to avoid introducing additional error.

600   With these identified limitations, continued research is needed to assess the biases in the

601   real-time precipitation retrievals on a local to regional basis so the assimilation system

602   can be modified accordingly.

603   The assimilation scheme used here assumed that the errors were attributed to the real-

604   time precipitation retrievals, but the precipitation estimates after adjustment includes

605   errors from additional sources. The two primary sources are errors in soil moisture

606   retrievals and errors in the land surface model that include model parameterizations

607   (poorly or insufficiently represented processes as well as scale issues) and parameter

608   errors (insufficient calibration). There are also errors in other model forcing fields besides

609 precipitation. Further studies are needed to assess the attribution of these error sources to
610 the total error. Such research will further improve the use of real-time satellite-based
611 precipitation for global flood monitoring.

612 Besides the clear, heavy dependency of the assimilation effectiveness on the accuracy of
613 satellite soil moisture product, it is also important to acquire adequate knowledge on the
614 error characteristics of satellite soil moisture retrievals. Knowledge of the soil moisture
615 errors could be important and the assimilation methods (including precipitation ensemble
616 generation and pre-/post-processing method) should be chosen accordingly. On the other
617 hand, the presence of data gaps between overpasses could be a large source of uncertainty
618 with data assimilation. Further effort towards reliable spatial-temporal continuous (gap
619 filled) satellite soil moisture datasets is needed.

620 While it has been illustrated in this study that the enhancement of real time satellite
621 precipitation estimates can be realized through an assimilation approach using satellite
622 soil moisture data products and a particle filter, additional satellite-based observations
623 (e.g. multi-sensor soil moisture products) or variables (e.g. land surface temperatures as
624 shown in Wanders et al. 2015, inundated areas), could be added/replaced in the
625 assimilation process with different levels of complexity; e.g. by applying constraints on
626 the particle generation. This opens up a great number of opportunities in using space-
627 borne observations for supplementing direct retrievals of precipitation.

628 **Acknowledgements**

634

635 **References**

636 Brocca, L., Melone, F., Moramarco, T. and Morbidelli, R.: Antecedent wetness

637 conditions based on ERS scatterometer data, J. Hydrol., 364(1-2), 73–87,

638 doi:10.1016/j.jhydrol.2008.10.007, 2009.

639 Brocca, L., Moramarco, T., Melone, F. and Wagner, W.: A new method for rainfall

640 estimation through soil moisture observations, Geophys. Res. Lett., 40(5), 853–858,

641 doi:10.1002/grl.50173, 2013.

642 Brocca, L., Ciabatta, L., Massari, C., Moramarco, T., Hahn, S., Hasenauer, S., Kidd, R.,

643 Dorigo, W., Wagner, W. and Levizzani, V.: Soil as a natural rain gauge: Estimating

644 global rainfall from satellite soil moisture data, J. Geophys. Res. Atmos., 119(9), 5128–

645 5141, doi:10.1002/2014JD021489, 2014.

646 Chopin, F., Berges, J., Desbois, M., Jobard, I. and Lebel, T.: Satellite Rainfall Probability

647 and Estimation. Application to the West Africa During the 2004 Rainy Season, AGU

648 Spring Meet. Abstr., A12, 2005.

649 Crow, W. T.: Correcting land surface model predictions for the impact of temporally

650 sparse rainfall rate measurements using an ensemble Kalman filter and surface brightness

651 temperature observations, J. Hydrometeorol., 4(5), 960–973, 2003.

652 Crow, W. T., Huffman, G. J., Bindlish, R. and Jackson, T. J.: Improving Satellite-Based

653 Rainfall Accumulation Estimates Using Spaceborne Surface Soil Moisture Retrievals, J.

654 Hydrometeorol., 10(1), 199–212, doi:10.1175/2008JHM986.1, 2009.

655 Crow, W. T., Van Den Berg, M. J., Huffman, G. J. and Pellarin, T.: Correcting rainfall

656 using satellite-based surface soil moisture retrievals: The Soil Moisture Analysis Rainfall

657 Tool (SMART), Water Resour. Res., 47(8), 1–15, doi:10.1029/2011WR010576, 2011.

658 Dee, D. P., Uppala, S. M., Simmons, A. J., Berrisford, P., Poli, P., Kobayashi, S., Andrae,

659 U., Balmaseda, M. A., Balsamo, G., Bauer, P. and others: The ERA-Interim reanalysis:

660 Configuration and performance of the data assimilation system, Q. J. R. Meteorol. Soc.,

661 137(656), 553–597, 2011.

662   Ebert, E. E., Janowiak, J. E. and Kidd, C.: Comparison of near-real-time precipitation

663   estimates from satellite observations and numerical models, Bull. Am. Meteorol. Soc.,

664   88(1), 47–64, doi:10.1175/BAMS-88-1-47, 2007.

665   Ek, M. B., Xia, Y., Wood, E., Sheffield, J., Luo, L., Lettenmaier, D., Livneh, B., Mocko,

666   D., Cosgrove, B., Meng, J., Wei, H., Koren, V., Schaake, J., Mo, K., Fan, Y. and Duan,

667   Q.: North American Land Data Assimilation System Phase 2 (NLDAS-2): Development

668   and Applications, GEWEX Newsl., 21(2), 5–7, 2011.

669   Francois, C., Quesney, A. and Ottlé, C.: SAR Data into a Coupled Land Surface–

670   Hydrological Model Using an Extended Kalman Filter, J. Hydrometeorol., 4(2), 473–487,

671   doi:10.1175/1525-7541(2003)4<473:SAOESD>2.0.CO;2, 2003.

672   Gao, H., Tang, Q., Shi, X., Zhu, C., Bohn, T. J., Su, F., She eld, J., Pan, M., and Wood,

673   E. F.: Water budget record from Variable Infiltration Capacity (VIC) model, in:

674   Algorithm Theoretical Basis Document for Terrestrial Water Cycle Data Records (in

675   review), 2010.

676   Huffman, G. J., Bolvin, D. T., Nelkin, E. J., Wolff, D. B., Adler, R. F., Gu, G., Hong, Y.,

677   Bowman, K. P. and Stocker, E. F.: The TRMM Multisatellite Precipitation Analysis

678   (TMPA): Quasi-Global, Multiyear, Combined-Sensor Precipitation Estimates at Fine

679   Scales, J. Hydrometeorol., 8(1), 38–55, doi:10.1175/JHM560.1, 2007.

680   Huffman, G. J., Adler, R. F., Bolvin, D. T., and Nelkin, E. J.: The TRMM Multi-satellite

681   Precipitation Analysis (TMPA), in: Satellite Rainfall Applications for Surface

682   Hydrology, Springer Netherlands, 3–22, 2010.

683   Kalman, R. E.: A New Approach to Linear Filtering and Prediction Problems, J. Basic

684   Eng., 82(1), 35, doi:10.1115/1.3662552, 1960.

685   Kerr, Y. H., Waldteufel, P., Richaume, P., Wigneron, J.-P., Ferrazzoli, P., Mahmoodi, A.,

686   Al Bitar, A., Cabot, F., Gruhier, C., Juglea, S. E., Leroux, D., Mialon, A. and Delwart, S.:

687   The SMOS Soil Moisture Retrieval Algorithm, Geosci. Remote Sensing, IEEE Trans.,

688   50(5), 1384–1403, doi:10.1109/TGRS.2012.2184548, 2012.

689 Liang, X., Lettenmaier, D. P., Wood, E. F. and Burges, S. J.: A simple hydrologically
690 based model of land surface water and energy fluxes for general circulation models, J.
691 Geophys. Res., 99, 14415–14428, doi:10.1029/94JD00483, 1994.

692 Liang, X., Wood, E. F. and Lettenmaier, D. P.: Surface soil moisture parameterization of
693 the VIC-2L model: Evaluation and modification, Glob. Planet. Change, 13(1-4), 195–
694 206, doi:10.1016/0921-8181(95)00046-1, 1996.

695 Massari, C., Brocca, L., Moramarco, T., Tramblay, Y. and Didon Lescot, J.-F.: Potential
696 of soil moisture observations in flood modelling: estimating initial conditions and
697 correcting rainfall, Adv. Water Resour., 74, 44–53, doi:10.1016/j.advwatres.2014.08.004,
698 2014.

699 Matgen, P., Fenicia, F., Heitz, S., Plaza, D., de Keyser, R., Pauwels, V. R. N., Wagner,
700 W. and Savenije, H.: Can ASCAT-derived soil wetness indices reduce predictive
701 uncertainty in well-gauged areas? A comparison with in situ observed soil moisture in an
702 assimilation application, Adv. Water Resour., 44, 49–65,
703 doi:10.1016/j.advwatres.2012.03.022, 2012.

704 McCabe, M. F., Wood, E. F. and Gao, H.: Initial soil moisture retrievals from AMSR-E:
705 Multiscale comparison using in situ data and rainfall patterns overs Iowa, Geophys. Res.
706 Lett., 32(6), 1–4, doi:10.1029/2004GL021222, 2005.

707 Pan, M. and Wood, E. F.: Data Assimilation for Estimating the Terrestrial Water Budget
708 Using a Constrained Ensemble Kalman Filter, J. Hydrometeorol., 7(3), 534–547,
709 doi:10.1175/JHM495.1, 2006.

710 Pan, M., Li, H. and Wood, E.: Assessing the skill of satellite-based precipitation
711 estimates in hydrologic applications, Water Resour. Res., 46(9), W09535,
712 doi:10.1029/2009WR008290, 2010.

713 Pan, M., Sahoo, A. K. and Wood, E. F.: Improving soil moisture retrievals from a
714 physically-based radiative transfer model, Remote Sens. Environ., 140, 130–140,
715 doi:10.1016/j.rse.2013.08.020, 2014.

716 Pellarin, T., Ali, A., Chopin, F., Jobard, I. and Bergès, J. C.: Using spaceborne surface
717 soil moisture to constrain satellite precipitation estimates over West Africa, Geophys.
718 Res. Lett., 35(2), 3–7, doi:10.1029/2007GL032243, 2008.

719 Pellarin, T., Louvet, S., Gruhier, C., Quantin, G. and Legout, C.: A simple and effective
720 method for correcting soil moisture and precipitation estimates using AMSR-E
721 measurements, Remote Sens. Environ., 136, 28–36, doi:10.1016/j.rse.2013.04.011, 2013.

722 Robock, A., Luo, L., Wood, E. F., Wen, F., Mitchell, K., Houser, P., Schaake, J.,
723 Lohmann, D., Cosgrove, B., Sheffield, J., Duan, Q., Higgins, W., Pinker, R., Tarpley, D.,
724 Basara, J. and Crawford, K.: Evaluation of the North American Land Data Assimilation
725 System over the southern Great Plains during the warm season, J. Geophys. Res.,
726 108(D22), 8846, doi:10.1029/2002JD003245, 2003.

727 Schaake, J. C., Duan, Q., Koren, V., Mitchell, K. E., Houser, P. R., Wood, E. F., Robock,
728 A., Lettenmaier, D. P., Lohmann, D., Cosgrove, B., Sheffield, J., Luo, L., Higgins, R. W.,
729 Pinker, R. T. and Tarpley, J. D.: An intercomparison of soil moisture fields in the North
730 American Land Data Assimilation System (NLDAS), J. Geophys. Res. Atmos., 109(D1),
731 doi:10.1029/2002JD003309, 2004.

732 Schamm, K., M. Ziese, A. Becker, P. Finger, A. Meyer-Christoffer, U. Schneider, M.
733 Schröder, and P. Stender (2014), Global gridded precipitation over land: A description of
734 the new GPCC First Guess Daily product, *Earth Syst. Sci. Data*,6,49–60

735 Sorooshian, S.: Commentary-GEWEX (Global Energy and Water Cycle Experiment) at
736 the 2004 Joint Scientific Committee Meeting, GEWEX Newsl., 14(2), 2, 2004.

737 Wanders, N., Pan, M. and Wood, E. F.: Correction of real-time satellite precipitation with
738 multi-sensor satellite observations of land surface variables, Remote Sens. Environ., 160,
739 206–221, doi:10.1016/j.rse.2015.01.016, 2015.

740 Wu, H., Adler, R. F., Tian, Y., Huffman, G. J., Li, H. and Wang, J.: Real-time global
741 flood estimation using satellite-based precipitation and a coupled land surface and routing
742 model. Water Resour. Res., 50(3), 2693-2717, doi:10.1002/2013WR014710, 2014.

743 **List of Tables**

744 **Tables**

745 Table 1 Error statistics of recovered precipitation and effect of surface saturation in the idealized experiment (mm/day).

746 Table 2 Error statistics of recovered NLDAS based on ΔSM (with added errors) conditioned on 1st layer soil wetness for the idealized

747 experiment (mm/day).

748 Table 3 Error statistics of 3B42RT and 3B42RT$_{ADJ}$ compared to NLDAS precipitation (mm/day)

772   Figure 8 May 26th 2006 Rainfall pattern in 3B42RT (b) against NLDAS (d) as detected

773   by AMSR-E/LSMEM ΔSM (a), and recovered rainfall field (3B42RT$_{ADJ}$) by assimilating

774   AMSR-E/LSMEM ΔSM (c). Gray shading shows area without soil moisture retrievals.

775   Figure 9 Pearson correlation coefficient between AMSR-E/LSMEM ΔSM and

776   precipitation: a) NLDAS, b) 3B42RT and c) 3B42RT$_{ADJ}$; annual mean precipitation in d)

777   NLDAS, e) 3B42RT and f) 3B42RT$_{ADJ}$ of time steps with AMSR-E/LSMEM ΔSM

778   retrievals.

779   Figure 10 Frequency of rainy days in 3B42RT, 3B42RT$_{ADJ}$ and NLDAS with a) 0.1

780   mm/day and b) 2 mm/day rainfall threshold to define a rain day.

781   Figure 11 Distribution of 3B42RT and 3B42RT$_{ADJ}$ precipitation error compared to

782   NLDAS. Statistics are provided in Table 3.

783   Figure 12 FAR and POD of 3B42RT and 3B42RT$_{ADJ}$ with a) 0.1 mm/day and b) 2

784   mm/day rainfall threshold to define a rain event.

785   Figure 13 Probability that the added rainy days (3B42RT = 0 mm/day, 3B42RT$_{ADJ}$ > 0

786   mm/day) are true rain events (NLDAS > 0 mm/day) given corresponding AMSR-

787   E/LSMEM ΔSM.

788

Tables

Table 1 Error statistics of recovered precipitation and effect of surface saturation in the idealized experiment (mm/day).

[Recovered NLDAS]-[NLDAS]	[3B42RT]-[NLDAS]	0	0~0.2	0.2~0.5	0.5~1.0	1.0~1.5	1.5~2	2~2.5	2.5~5.0	5.0~7.5	7.5~10	10~15	15~20	20~25	>25
All surface	Bias	0.24	0.20	0.37	0.51	0.71	0.87	1.09	0.67	1.16	1.30	2.51	3.32	3.75	3.95
conditions	MAE	0.40	0.42	0.66	0.86	1.14	1.41	1.70	1.48	2.24	2.63	4.21	5.56	6.70	9.76
Unsaturated	Bias	0.23	0.19	0.29	0.40	0.52	0.68	0.82	0.65	1.10	1.27	2.19	2.88	3.14	3.14
surface	MAE	0.39	0.41	0.59	0.75	0.95	1.21	1.43	1.45	2.17	2.58	3.88	5.11	6.07	8.94
Saturated	Bias	2.31	5.06	47.65	42.58	50.67	44.09	59.64	6.83	16.09	9.19	46.47	57.98	65.33	64.09
surface	MAE	3.35	5.54	48.71	43.73	52.43	46.96	61.85	9.64	21.42	15.01	49.07	60.78	69.53	70.73

Table 2 Error statistics of recovered NLDAS based on ΔSM (with added errors) conditioned on 1st layer soil wetness for the idealized experiment (mm/day).

[Recovered NLDAS]–[NLDAS] [mm/day]	[VIC 1st layer SM] - [maximum]* [mm]	<-30	-30~-25	-25~-20	-20~-15	-15~-12	-12~-10	-10~-9	-9~-8	>-8
No error	Median	0.04	0.03	0.02	0.02	0.02	0.03	0.03	0.04	0.16
	IQR	0.14	0.08	0.07	0.07	0.08	0.12	0.21	0.29	1.71
1.0	Median	0.86	1.07	1.08	1.03	0.99	0.97	0.97	0.94	0.66
	IQR	1.52	1.72	1.77	1.83	1.96	2.08	2.14	2.19	2.59
2.0	Median	0.68	1.07	1.40	1.56	1.52	1.44	1.51	1.64	1.54
	IQR	1.76	2.09	2.88	3.45	3.63	3.73	3.73	3.73	3.91
3.0	Median	0.15	0.80	1.20	1.41	1.47	1.51	1.65	1.84	1.88
	IQR	1.36	2.16	3.04	3.73	3.74	3.79	4.34	5.24	5.47
4.0	Median	0.22	0.56	0.83	1.15	1.30	1.40	1.63	1.88	1.97
	IQR	0.99	2.36	2.48	3.99	4.05	4.70	5.53	5.52	5.63
5.0	Median	0.00	0.15	0.52	0.90	1.10	1.27	1.54	1.81	1.89
	IQR	1.62	2.54	2.91	4.43	4.51	5.95	5.90	5.79	7.04

*1st layer soil depth is 100mm with a SM capacity of ~45mm depending on porosity.

Table 3 Error statistics of 3B42RT and 3B42RT$_{ADJ}$ compared to NLDAS precipitation (mm/day)

[3B42RT] - [NLDAS] [mm/day]		<-25	-25~-20	-20~-15	-15~-10	-10~-5	-5~-2	-2~-0.5	-0.5~0.5	0.5~2	2~5	5~10	10~15	15~20	20~25	>25
[3B42RT] - [NLDAS]	Mean	-32.32	-22.19	-17.13	-12.09	-6.98	-3.22	-1.09	-0.02	1.11	3.20	6.87	11.96	16.97	21.95	27.35
	STD	8.52	1.42	1.42	1.42	1.39	0.85	0.43	0.12	0.43	0.84	1.37	1.39	1.37	1.38	2.08
[3B42RT$_{ADJ}$]- [NLDAS]	Mean	-31.24	-20.31	-14.79	-9.69	-4.81	-1.60	0.16	1.08	0.44	0.21	0.02	-0.06	0.00	-0.03	-0.12
	STD	11.03	6.40	6.12	5.34	4.08	2.73	1.88	1.18	1.86	2.29	2.60	2.91	3.01	2.74	2.41
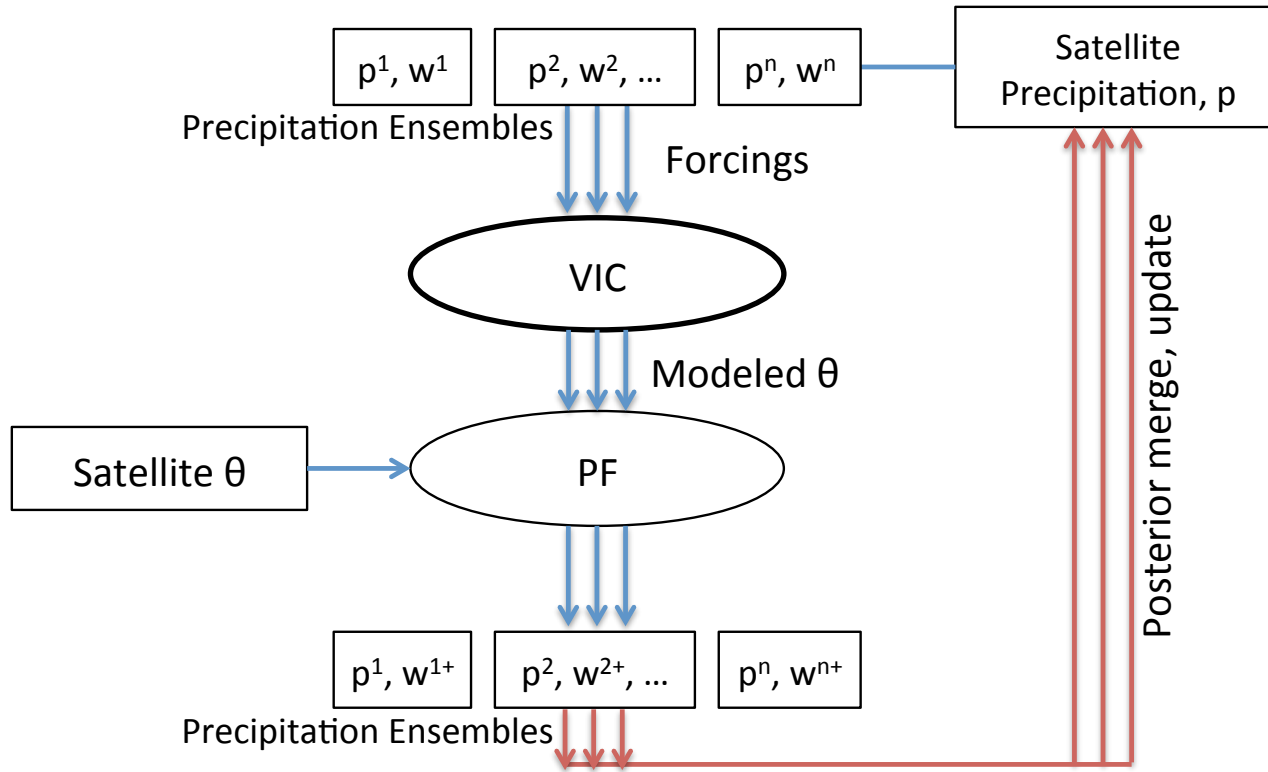
Figures

798   Figure 1 Schematic for the dynamic assimilation of AMSR-E/LSMEM ΔSM into TMPA (3B42RT) with the particle filter (PF).
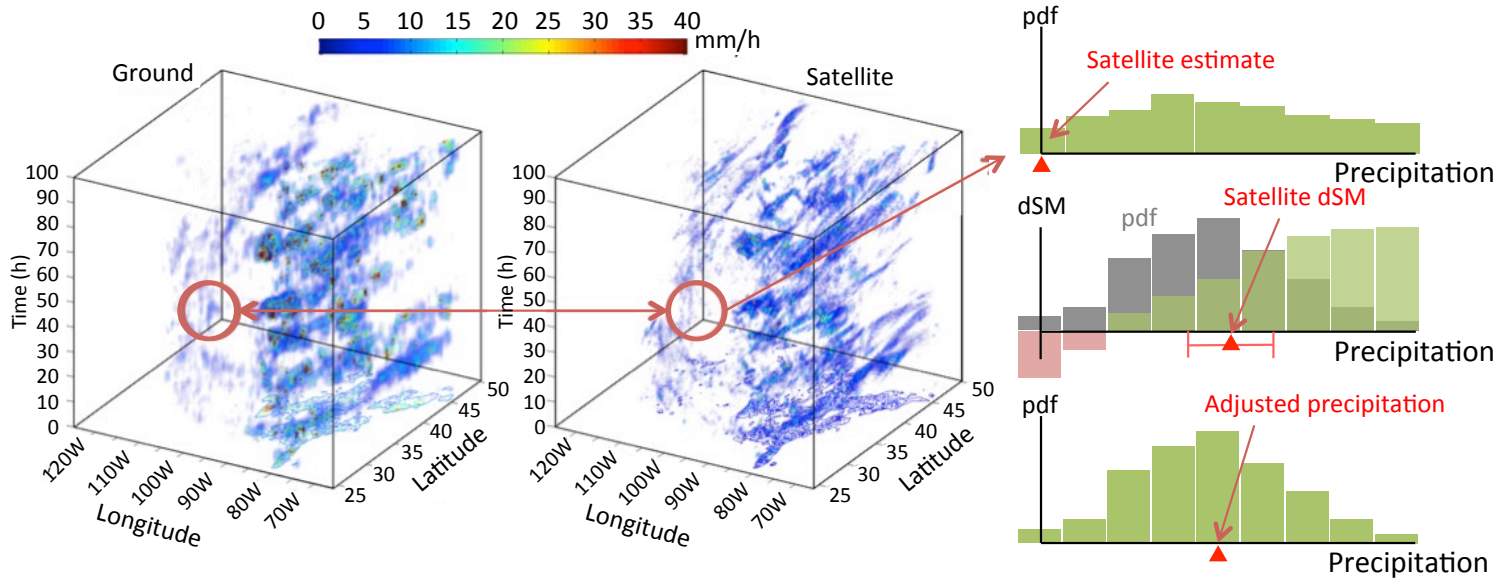
799

800   Figure 2 Schematic for the strategy for processing prior and posterior probability densities in the particle filter.
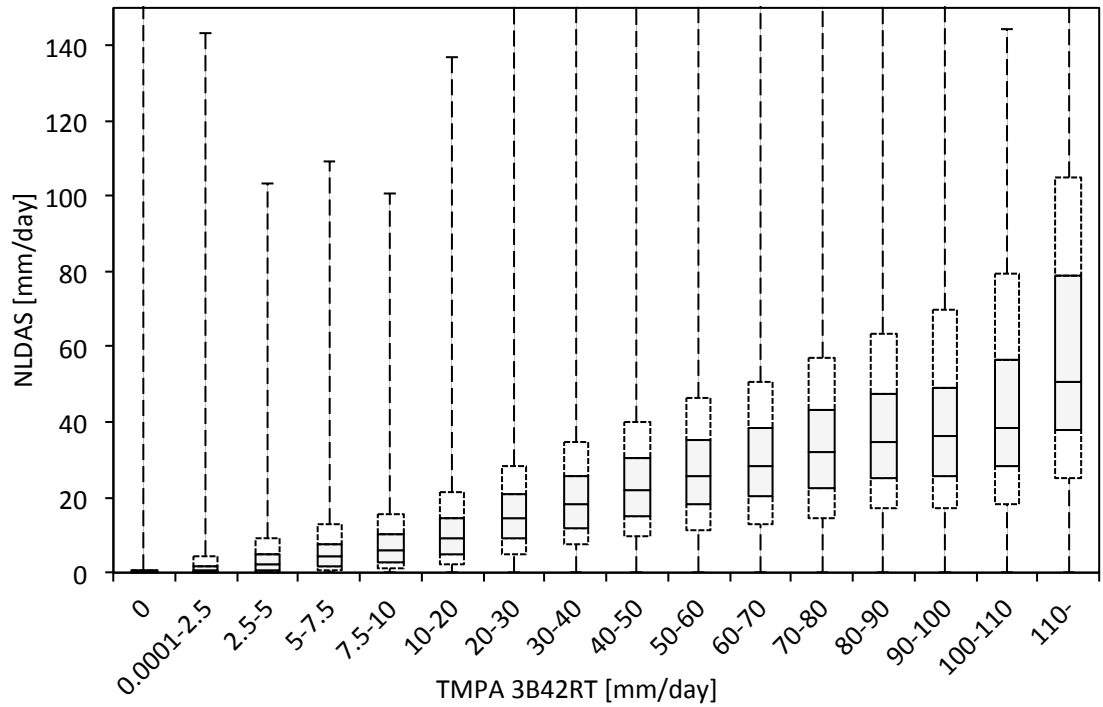
801

802 Figure 3 Statistics of NLDAS precipitation given 3B42RT precipitation measurement. Boxplot shows the minimum, 15% quantile,

803 30% quantile, median, 70% quantile, 85% quantile and maximum value of NLDAS precipitation given 3B42RT precipitation in a

804 certain bin.

805
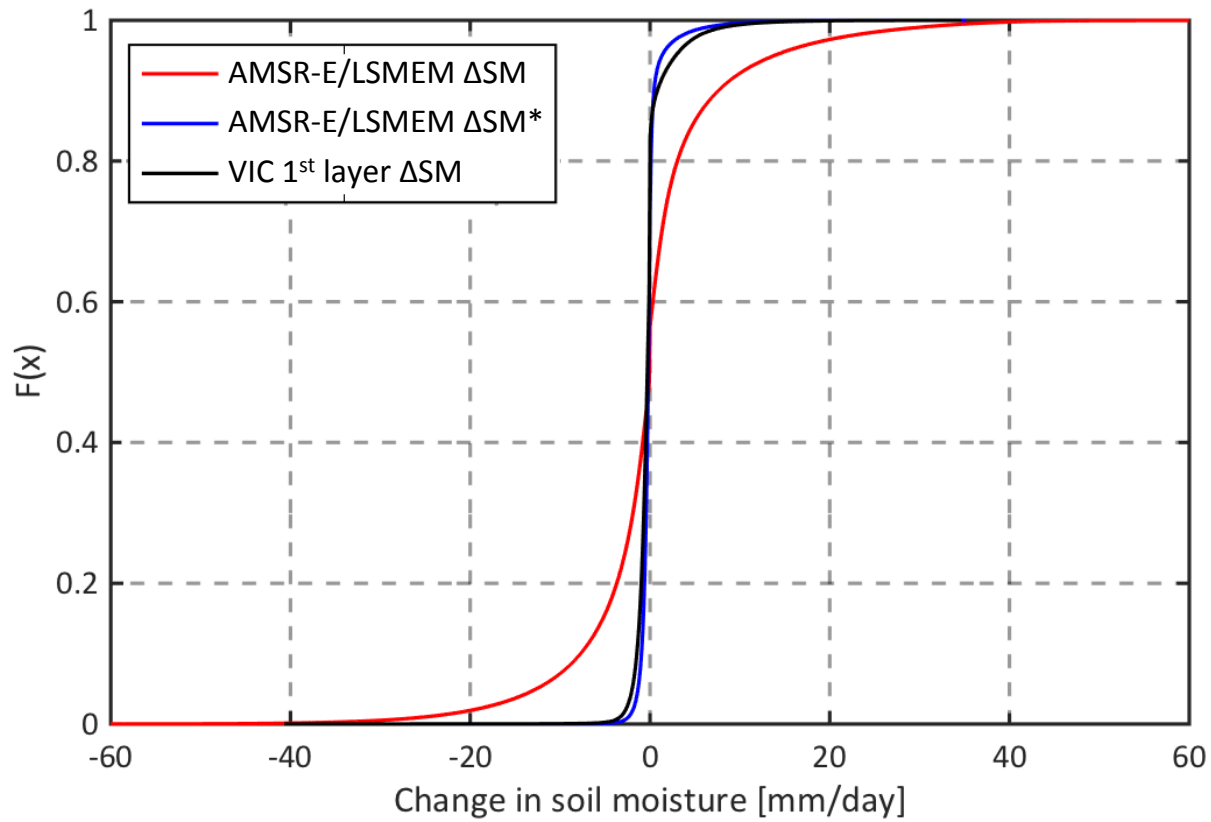
Figure 4 Empirical cumulative distribution function of changes in soil moisture from top layer soil moisture from NLDAS
precipitation forced VIC simulation (black), and AMSR-E/LSMEM soil moisture retrieval before (red) and after (blue) pre-
processing.

309
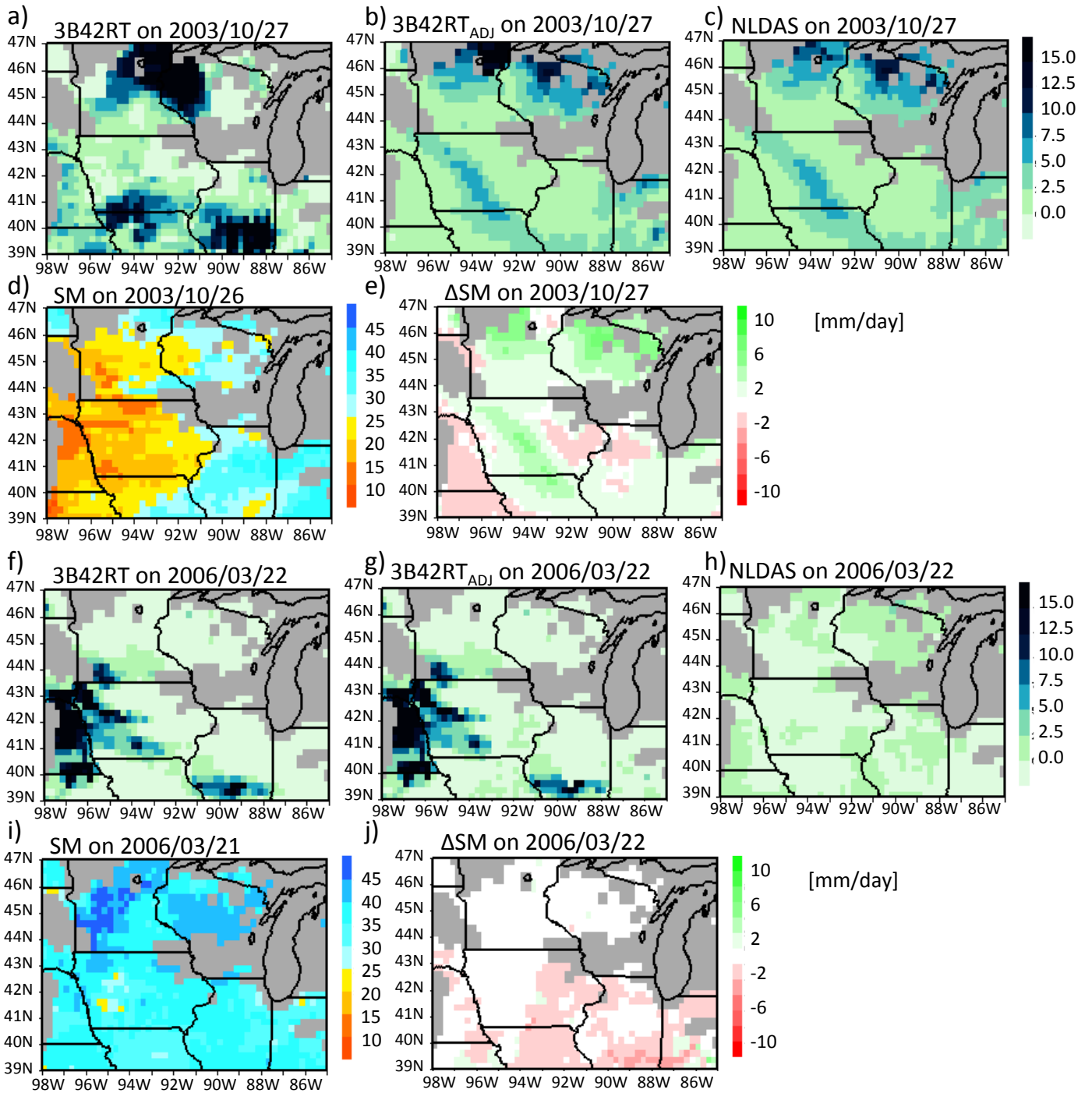
Figure 5 Two cases with recovered spatial rainfall pattern in the idealized experiment after merging satellite

310

soil moisture retrieval on: (a-e) 27th Oct. 2003 and (f-j) 22th Mar. 2006.

311
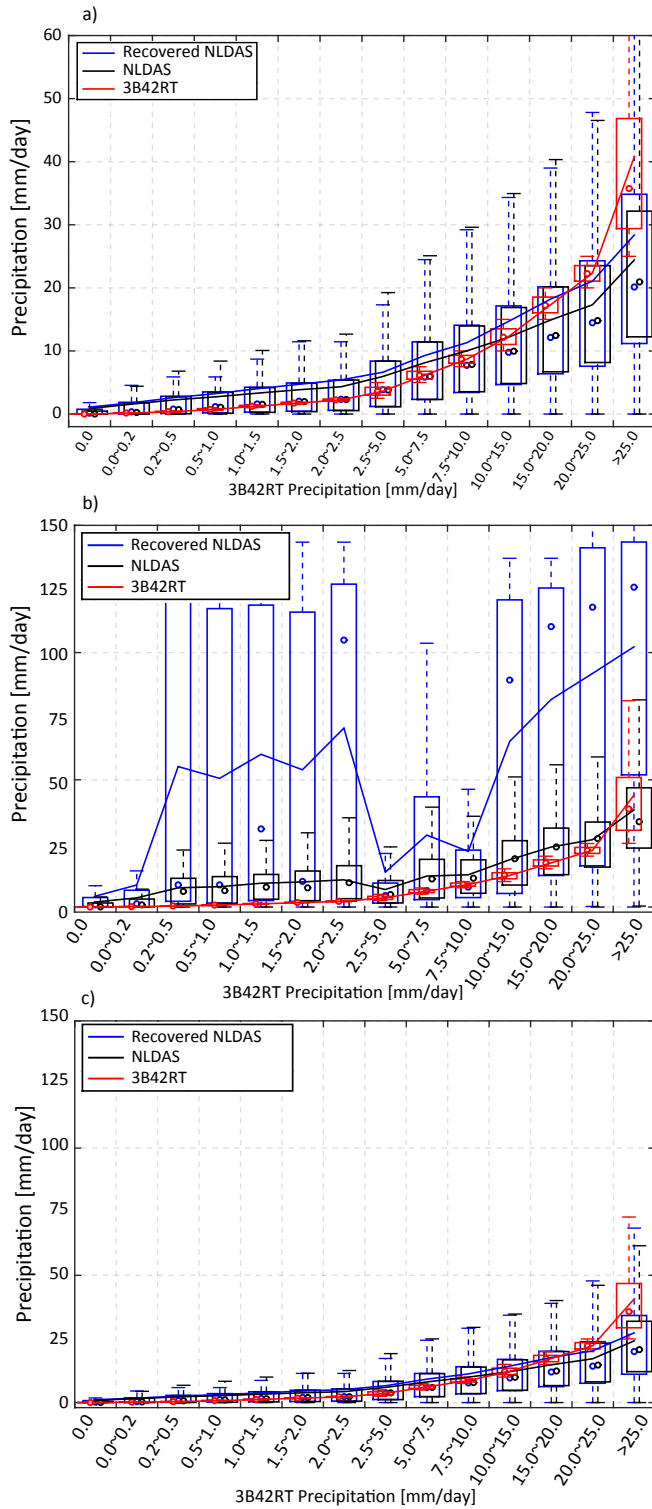
Figure 6 Accuracy of recovered precipitation in idealized experiment: (a) overall performance and separately comparing the improvement performance of recovered NLDAS precipitation (b) with and (c) without surface saturation condition. Statistics provided in Table 1.

312
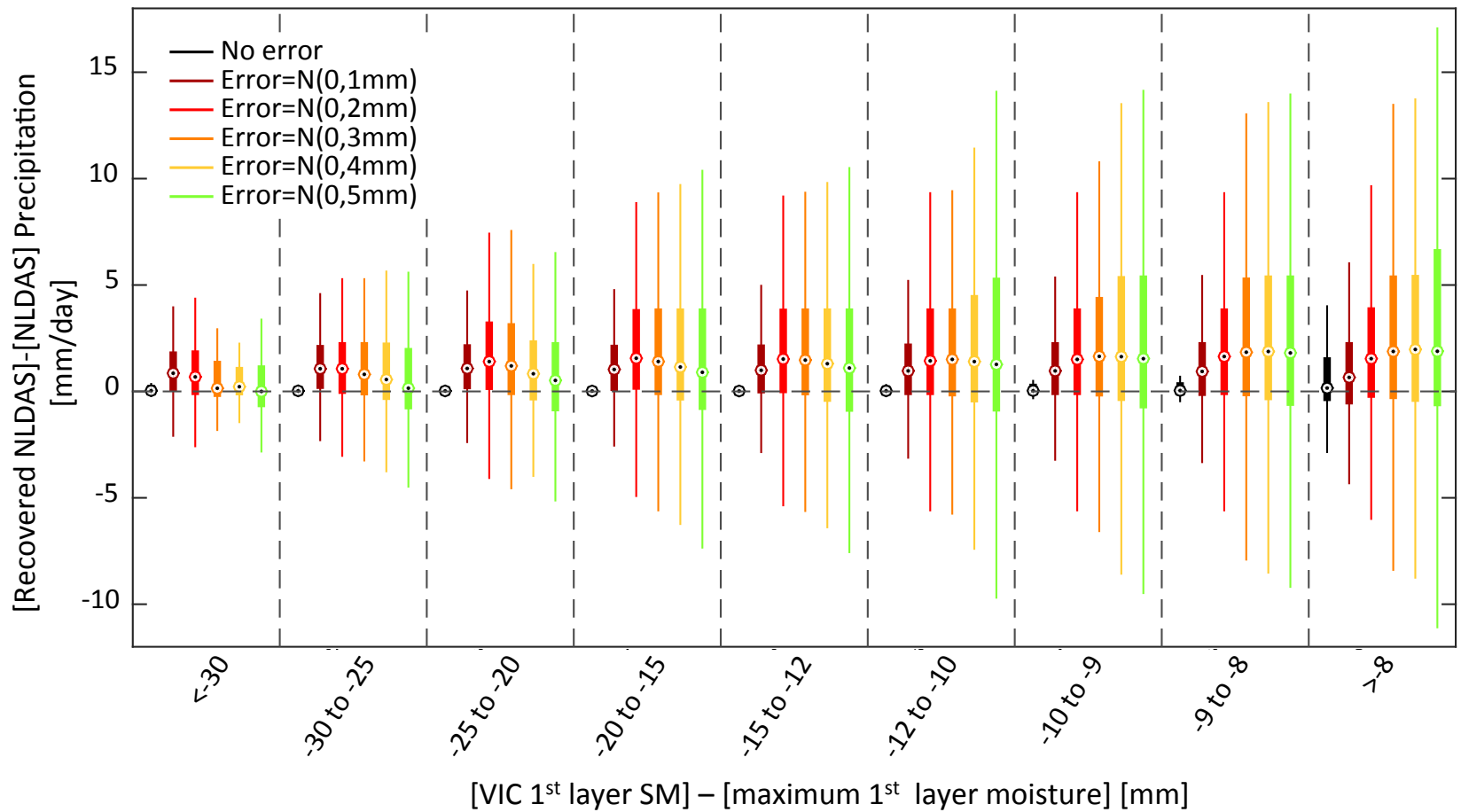
Figure 7 Error in recovered NLDAS precipitation given surface moisture condition. Recovered NLDAS is based on using "truth" soil moisture and soil moisture with normal error: N(0,1mm), N(0,2mm), N(0,3mm), N(0,4mm) and N(0,5mm). Statistics provided in Table 2.

817
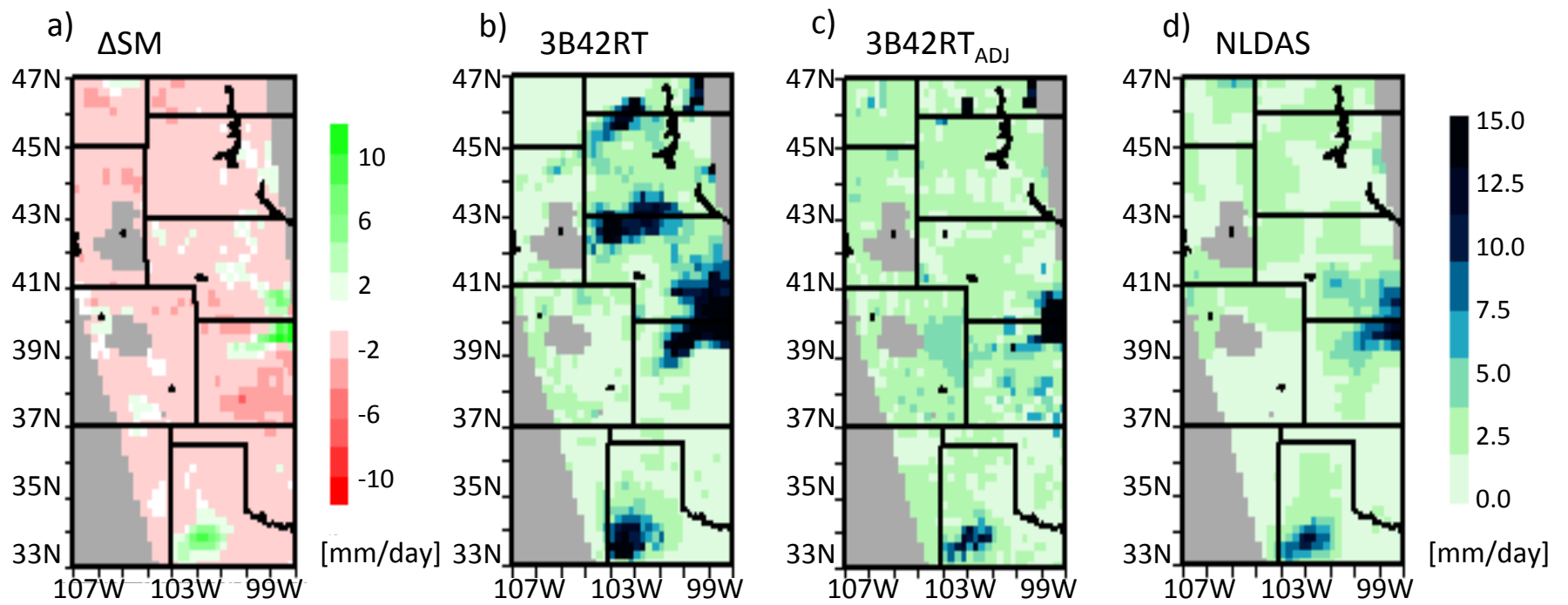
Figure 8 May 26th 2006 Rainfall pattern in 3B42RT (b) against NLDAS (d) as detected by AMSR-E/LSMEM ΔSM (a), and recovered
rainfall field (3B42RT$_{ADJ}$) by assimilating AMSR-E/LSMEM ΔSM (c). Gray shading shows area without soil moisture retrievals.
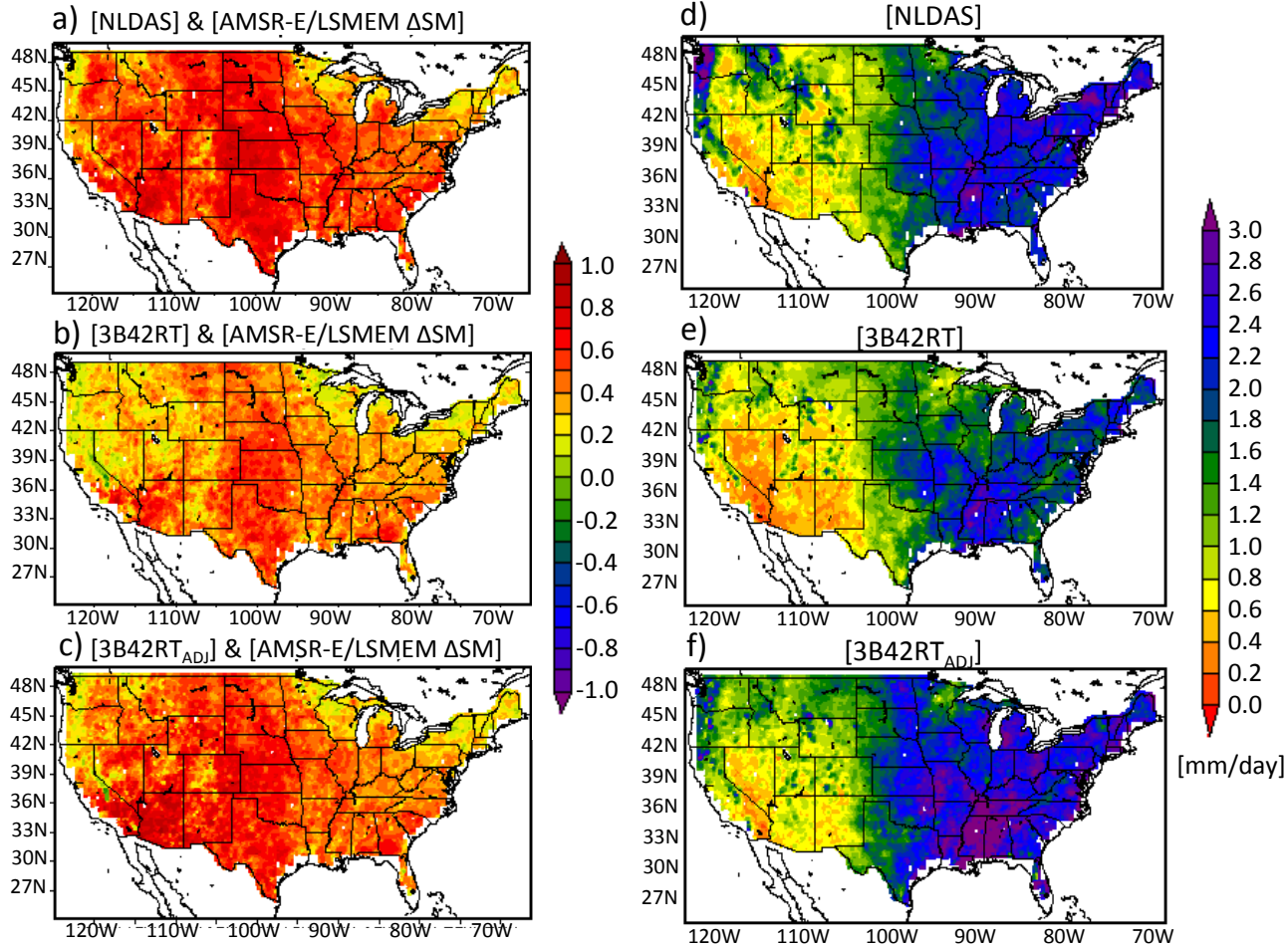
Figure 9 Pearson correlation coefficient between AMSR-E/LSMEM ΔSM and precipitation: a) NLDAS, b) 3B42RT and c) 3B42RT$_{ADJ}$; annual mean precipitation in d) NLDAS, e) 3B42RT and f) 3B42RT$_{ADJ}$ of time steps with AMSR-E/LSMEM ΔSM retrievals.
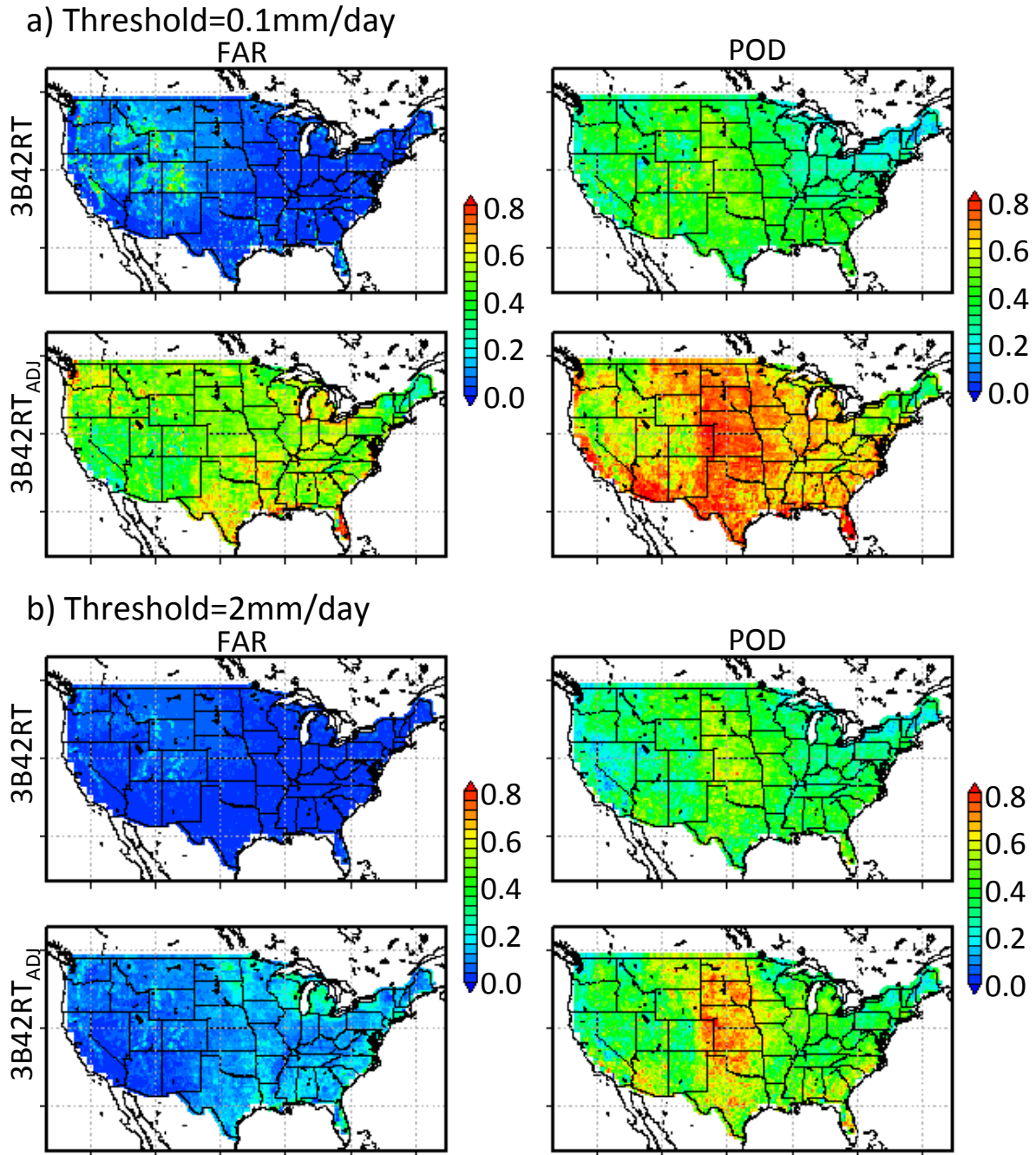
824
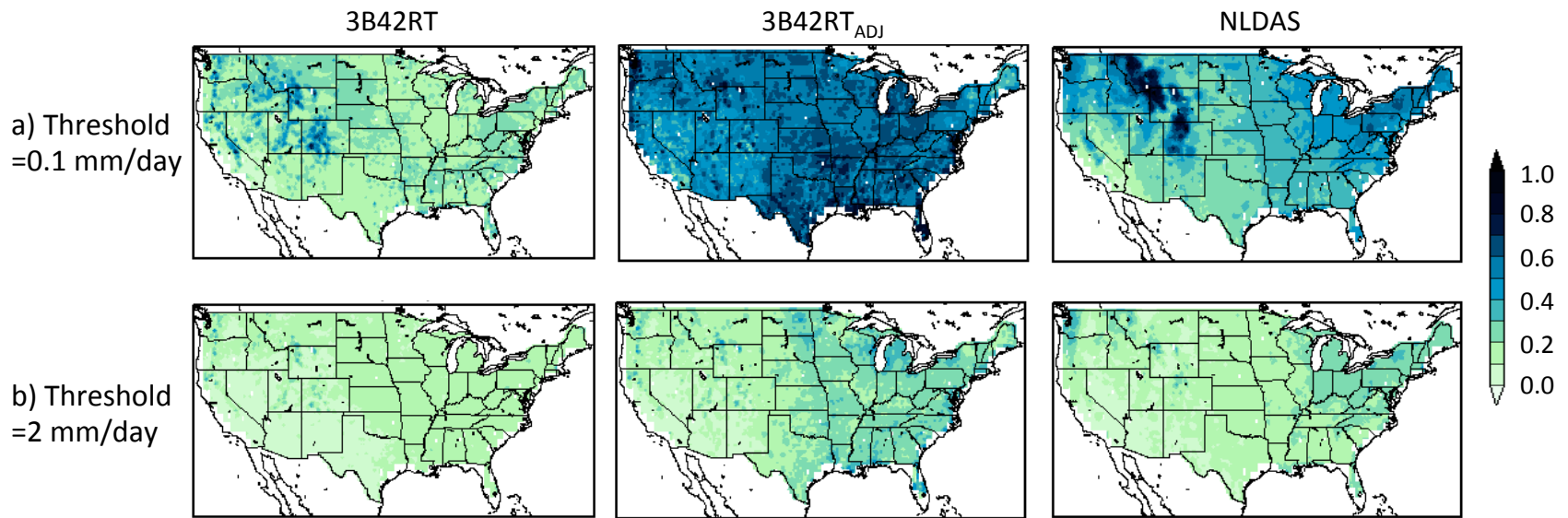
Figure 10 Frequency of rainy days in 3B42RT, 3B42RT$_{ADJ}$ and NLDAS with a) 0.1 mm/day and b) 2 mm/day rainfall threshold to
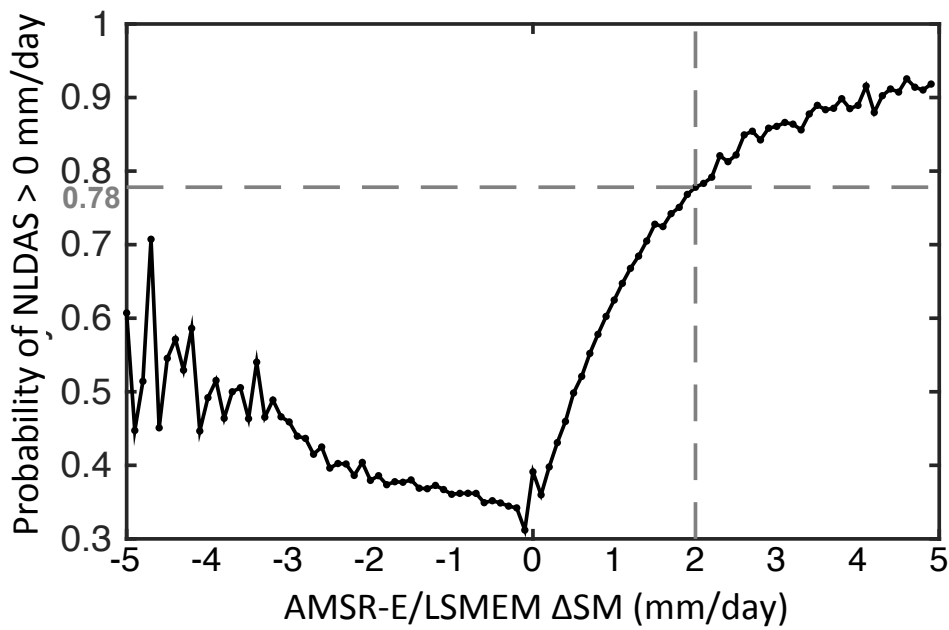
define a rain day.
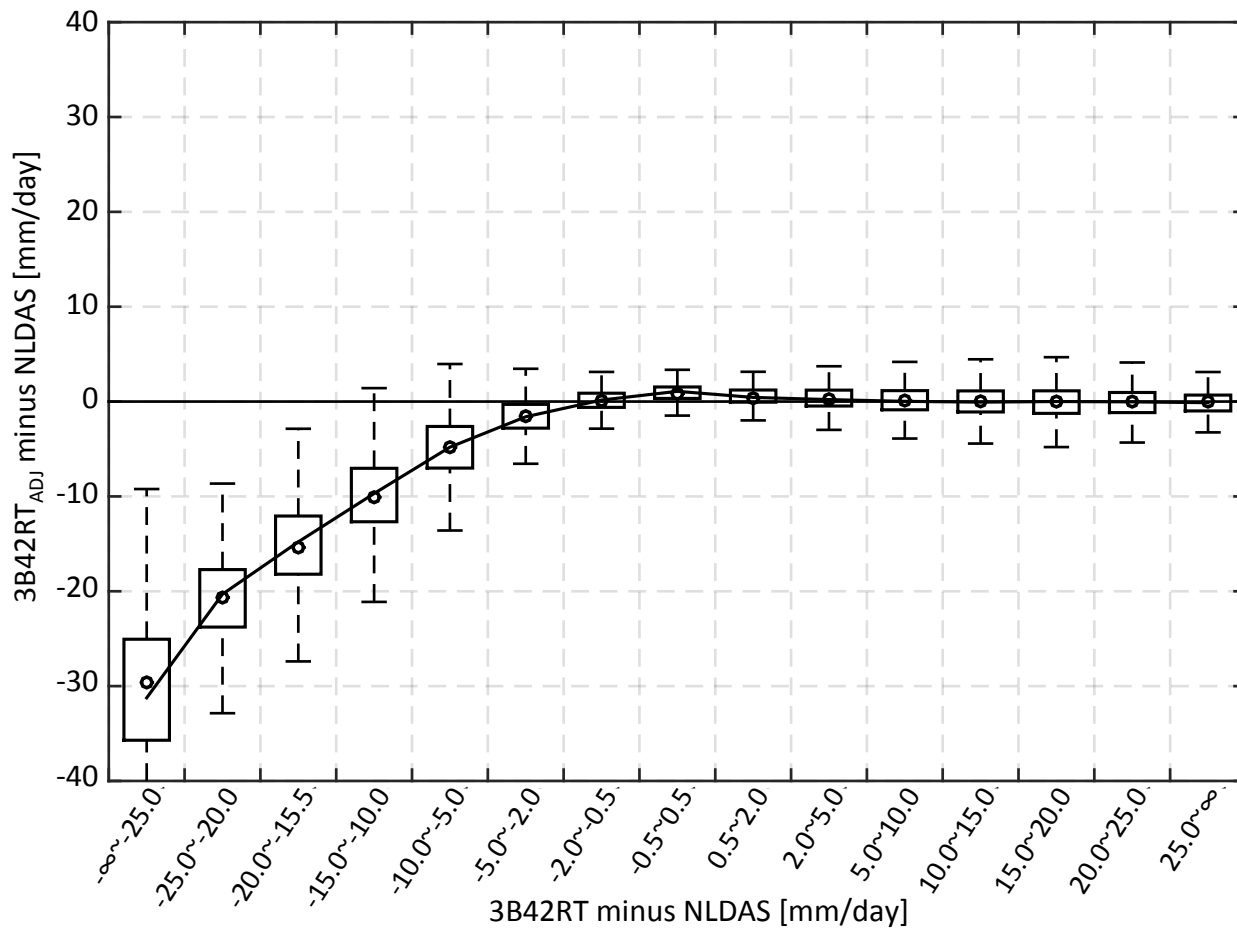
827

828   Figure 11 Distribution of 3B42RT and 3B42RT$_{ADJ}$ precipitation error compared to NLDAS. Statistics are provided in Table 3.

Figure 12 FAR and POD of 3B42RT and 3B42RT$_{ADJ}$ with a) 0.1 mm/day and b) 2 mm/day rainfall threshold to define a rain event.

832

Figure 13 Probability that the added rainy days (3B42RT = 0 mm/day, $3B42RT_{ADJ}$ > 0 mm/day) are

true rain events (NLDAS > 0 mm/day) given corresponding AMSR-E/LSMEM ΔSM.

835